Erstgutachterin: PD Dr. Jeanette Lorenz
Zweitgutachter: Prof. Dr. Wolfgang Dünnweber

Search for electroweakinos with the ATLAS detector

Thesis submitted for a doctoral degree in physics
at the faculty of physics of the
Ludwig-Maximilians University
Munich, Germany

Submitted by Eric Schanet, born in Luxembourg
on May 4th, 2021

Supported by the Luxembourg National Research Fund (FNR) (13562317)

Part I

Fundamental concepts

Part II

The 1-lepton analysis

Chapter 8

Results

This chapter discusses the results of the different profile likelihood fits to data and the hypothesis tests performed in the 1ℓ analysis. After the background estimation, obtained by a background-only fit in the control regions, is validated in the validation regions, the signal regions are unblinded and the observed data is compared to the Standard Model (SM) background expectation.

8.1 Background-only fit results

8.1.1 Results in the control regions

As all CRs are mutually exclusive, a background-only fit simultaneously using information from all CRs can be run. Only the terms related to the CRs enter the likelihood and any signal contamination present in the CRs is suppressed. This allows to fit the dominant backgrounds to data, and thus, by construction, leads to a good agreement between observed data and the total fitted background estimate in all CRs. The best-fit values and uncertainties of the free normalisation parameters for $t\bar{t}$ (μ_{T}), single top (μ_{ST}) and W + jets (μ_{W}) are determined after fit to be

$$\begin{aligned} \mu_{\mathrm{T}} &= 1.02^{+0.07}_{-0.09}, \\ \mu_{\mathrm{ST}} &= 0.6^{+0.5}_{-0.25}, \\ \mu_{\mathrm{W}} &= 1.22^{+0.26}_{-0.24}. \end{aligned} \tag{8.1}$$

While the dominant $t\bar{t}$ background stays roughly at its nominal expectation with respect to MC simulation, W + jets processes are slightly scaled up, and the single top expectation is scaled down. The high uncertainty on μ_{ST} can be attributed to the relatively low MC statistics and comparably low purity of single top events in STR.

Table 8.1 summarises the background estimates including all uncertainties for all control regions after the fit to data. As discussed in chapter 6, $t\bar{t}$ dominates in all control regions (except WR), followed by single top and W + jets processes. In WR, W + jets is the largest background, followed by $t\bar{t}$ processes. Due to the relatively small normalisation factor for single top processes, $t\bar{t}$ and single top processes contribute to roughly equal amounts to STR. Small contributions come from diboson, multiboson and other backgrounds like $t\bar{t}+V$, $t\bar{t}+h$ and $V+h$ production. All processes directly estimated from MC simulation cumulatively account for only 10%, 5.5% and a maximum of 2.6% in the single top, W + jets

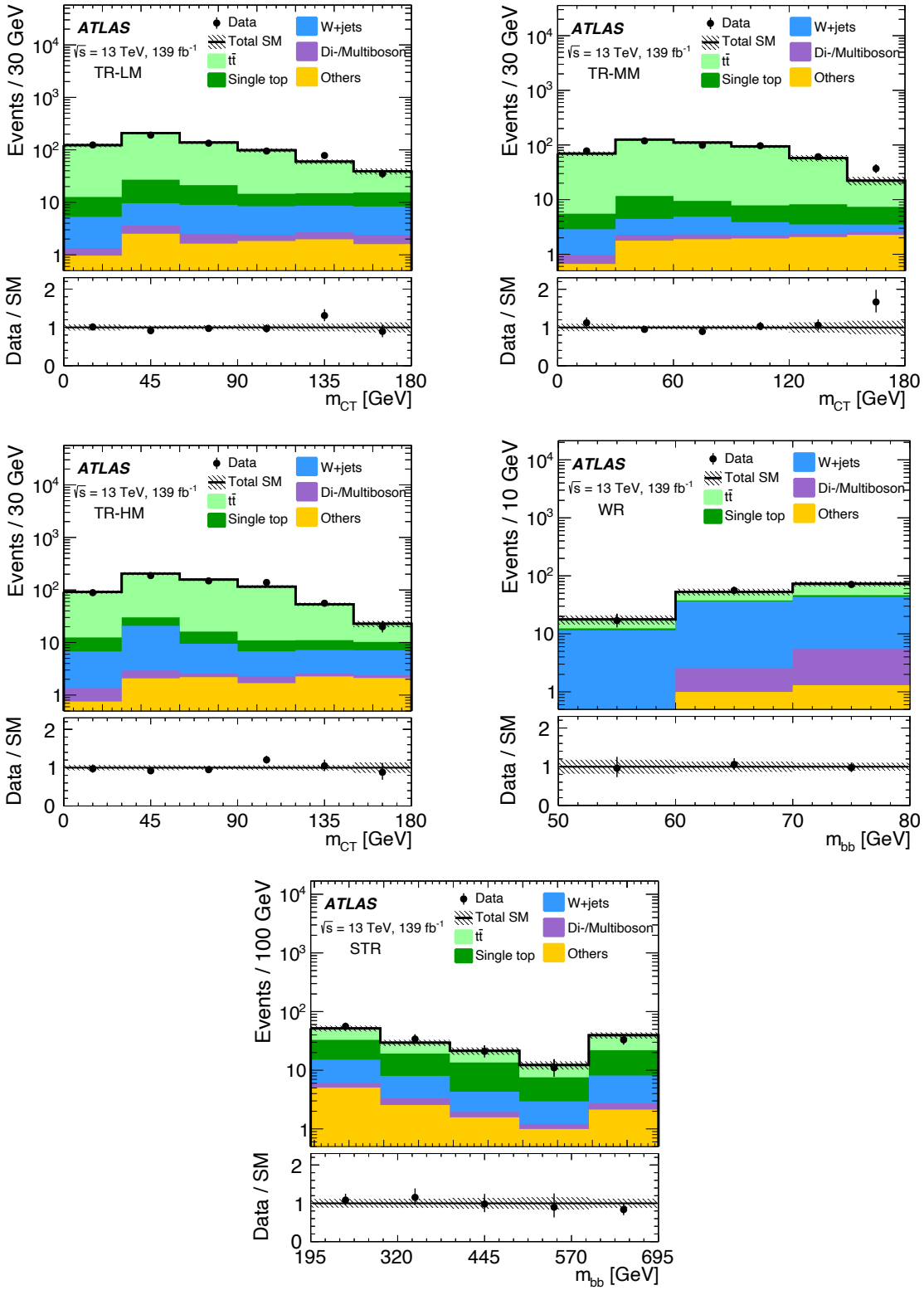

Figure 8.1: Exemplary distribution shown in each control region after the background-only fit. The shaded region includes all systematic uncertainties as well as Monte Carlo (MC) statistical uncertainty. The $t\bar{t}$, single top and W + jets are simultaneously normalised to data in all control regions (CRs). A good agreement between MC expectation and data is observed in all CRs. Adapted from Ref. [185].

Table 8.1: Background-only fit results for the CRs for an integrated luminosity of 139 fb^{-1}. Nominal MC expectations (normalised to MC cross-sections) are given for comparison. The errors shown include the MC statistical and systematic uncertainties.

Region	TR-LM	TR-MM	TR-HM	WR	STCR
Observed events	657	491	641	144	155
Fitted SM events	666 ± 25	480 ± 21	645 ± 26	143 ± 12	154 ± 15
$t\bar{t}$	560 ± 40	430 ± 33	550 ± 40	47 ± 9	59 ± 12
Single top	60 ± 40	27 ± 23	33 ± 27	5 ± 4	57 ± 22
W + jets	34 ± 8	10.5 ± 2.8	44 ± 11	83 ± 16	23 ± 6
Di-/Multiboson	4.3 ± 1.2	2.0 ± 0.5	2.8 ± 0.5	5.7 ± 1.0	2.8 ± 0.9
Other	10.5 ± 1.3	10.6 ± 1.4	11.1 ± 1.4	2.4 ± 0.4	12.3 ± 1.5
MC exp. SM events	720 ± 80	474 ± 33	680 ± 50	130 ± 13	180 ± 50
$t\bar{t}$	570 ± 70	407 ± 30	570 ± 40	46 ± 10	52 ± 10
Single top	102 ± 18	46 ± 13	58 ± 16	9 ± 6	90 ± 40
W + jets	29 ± 4	8.4 ± 1.2	36.1 ± 3.1	67 ± 5	19.0 ± 2.0
Di-/Multiboson	4.1 ± 1.1	2.0 ± 0.5	2.8 ± 0.5	5.6 ± 1.0	2.8 ± 0.9
Other	10.6 ± 1.3	10.6 ± 1.4	11.2 ± 1.4	2.5 ± 0.4	12.4 ± 1.5

and $t\bar{t}$ control regions, respectively. Exemplary distributions in the CRs after the background-only fit are shown in fig. 8.1, revealing a good agreement between observed data and the SM background estimate.

8.1.2 Results in the validation regions

In order to validate the extrapolations from the CRs to the signal regions (SRs), the results of the background-only fit in the CRs are first validated in the VRs. Table 8.2 summarises the observed data and SM background estimate in the different VR bins before and after the background-only fit in the CRs. Exemplary N-1 distributions in m_{CT} in all validation regions are shown in fig. 8.2.

In the on-peak VRs, designed to validate the extrapolation from the control regions over the $m_{b\bar{b}}$ distribution, $t\bar{t}$ is by far the most dominant background after the background-only fit. Contributions from single top and W + jets processes each amount to only 1–5%, depending on the validation region bin. Diboson, multiboson and other SM processes result in minor contributions of the level of not more than 3% of the total background estimate. As the total uncertainties on the background estimate in the on-peak regions are dominated by the $t\bar{t}$ uncertainties, the sizeable uncertainties on the W + jets and single top estimates due to relatively limited MC statistics do not have a significant impact.

After the background-only fit, $t\bar{t}$ is the dominant process in the low mass off-peak VRs, where contributions from single top and W + jets processes are subdominant. In the medium and high mass regimes, $t\bar{t}$, single top and W + jets production all result in similar contributions. Diboson, multiboson and other SM processes are only minor backgrounds in all off-peak regions, cumulatively amounting to only 10–14% of the total background estimate, depending on the mass regime.

The agreement between data and the background estimate is summarised in fig. 8.4. In VR-onMM and and VR-onHM, light overfluctuations with a significance [180] of 1.3σ and 1.7σ, respectively, are

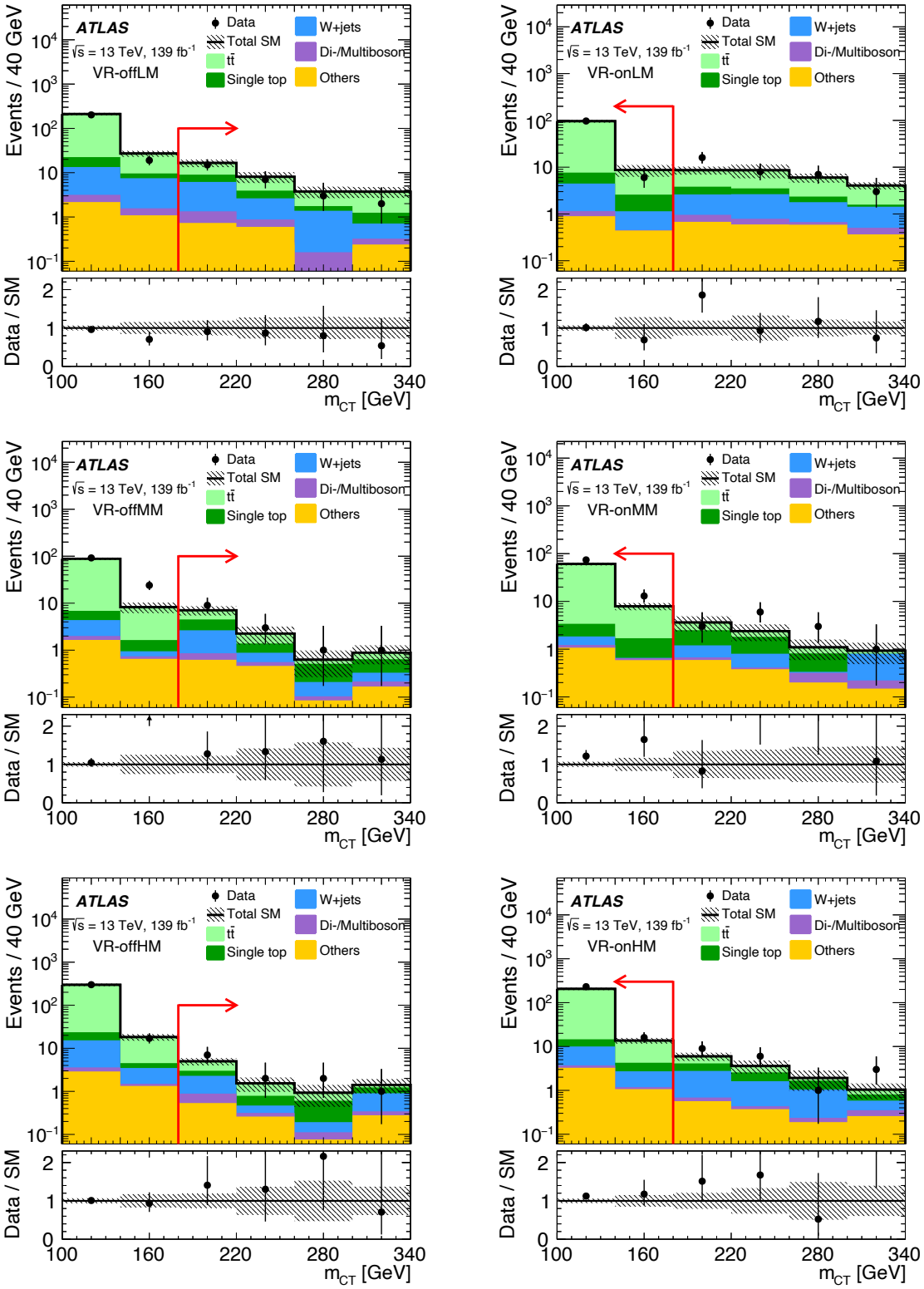

Figure 8.2: Exemplary $N-1$ distributions shown in each validation region after the background-only fit with subsequent extrapolation to the validation regions (VRs). All selection cuts except for the requirement on m_{CT} (indicated using the red arrow) are applied. The shaded region includes all systematic uncertainties as well as MC statistical uncertainty. Adapted from Ref. [185].

Table 8.2: Background-only fit results from the CRs extrapolated to the VRs for an integrated luminosity of 139 fb^{-1}. Nominal MC expectations (normalised to MC cross-sections) are given for comparison. The errors shown include the MC statistical and systematic uncertainties. Uncertainties in the fitted event rates are symmetric by construction, except where the negative error is truncated at an event rate of zero.

Region	VR-onLM	VR-onMM	VR-onHM	VR-offLM	VR-offMM	VR-offHM
Observed events	103	87	247	27	14	12
Fitted SM events	100 ± 19	64 ± 9	215 ± 18	34 ± 6	9.5 ± 2.7	7.5 ± 2.6
$t\bar{t}$	90 ± 19	59 ± 9	196 ± 19	18 ± 4	2.4 ± 1.4	1.8 ± 1.8
Single top	5^{+5}_{-5}	$2.6^{+2.9}_{-2.6}$	6 ± 6	5 ± 4	3.0 ± 1.8	1.8 ± 1.5
W + jets	4 ± 4	0.6 ± 0.5	7.9 ± 2.1	8.2 ± 2.6	2.3 ± 0.8	2.2 ± 0.6
Di-/Multiboson	0.24 ± 0.08	0.19 ± 0.08	0.54 ± 0.19	1.07 ± 0.27	0.39 ± 0.11	0.51 ± 0.14
Other	1.34 ± 0.22	1.67 ± 0.28	4.4 ± 2.0	1.6 ± 0.5	1.34 ± 0.25	1.15 ± 0.24
MC exp. SM events	110 ± 40	69 ± 17	218 ± 22	34 ± 7	12.8 ± 3.4	9.7 ± 3.3
$t\bar{t}$	92 ± 35	62 ± 17	196 ± 21	16 ± 5	3.8 ± 2.2	3.1 ± 1.9
Single top	8 ± 5	4.5 ± 3.4	11 ± 6	9 ± 4	5.3 ± 2.2	3.1 ± 2.5
W + jets	2.8 ± 2.3	0.5 ± 0.5	6.5 ± 1.2	6.5 ± 1.6	2.0 ± 0.5	1.80 ± 0.34
Di-/Multiboson	0.24 ± 0.07	0.19 ± 0.08	0.50 ± 0.17	1.07 ± 0.28	0.37 ± 0.10	0.50 ± 0.15
Other	1.35 ± 0.23	1.70 ± 0.28	4.4 ± 0.9	1.6 ± 0.5	1.36 ± 0.25	1.16 ± 0.24

observed in data. In the remaining VRs, the agreement between observed data and SM expectation is within 1σ. The overall agreement in the validation regions is thus considered to be acceptable, paving the way for further extrapolation of the background estimate into the SRs.

8.1.3 Results in the signal regions

By extrapolating the results from the background-only fit in the control regions, the background estimate in the signal regions can be obtained. In the following, the results in all discovery and exclusion signal regions are discussed.

Table 8.3 compares the background estimate with the observed data for all discovery signal regions. In the low-mass discovery signal region, $t\bar{t}$ production is the dominant background, followed by W + jets and single top processes. At higher values of m_{T}, i.e. in the medium-mass discovery signal region, all three main SM backgrounds contribute to roughly equal amounts. In the high-mass signal region, W + jets production is the largest SM background, followed by single top and $t\bar{t}$ processes. In all discovery signal regions, diboson, multiboson and other SM backgrounds yield only minor contributions.

The results in the exclusion signal regions are shown in table 8.4. As for the discovery signal regions, $t\bar{t}$ production is the dominant background in the low-mass exclusion signal region bins SR-LM, while W + jets processes slightly dominate in the high-mass exclusion signal region bins SR-HM. The m_{CT} distributions of all three exclusion SRs are shown in fig. 8.3.

None of the exclusion or discovery signal regions reveal a significant deviation in data compared to the SM expectation, and all observations are in good agreement with the SM. A slight overfluctuation of data in the discovery SRs is quantified to have a significance of 1.8σ, 1.6σ and 1.2σ in the discovery

Table 8.3: Background-only fit results extrapolated to the discovery SRs for an integrated luminosity of 139 fb^{-1}. Nominal MC expectations (normalised to MC cross-sections) are given for comparison. The errors shown include the MC statistical and systematic uncertainties. Uncertainties in the fitted yields are symmetric by construction, except where the negative error is truncated at an event yield of zero.

Region	SR-LM (disc.)	SR-MM (disc.)	SR-HM (disc.)
Observed events	66	32	14
Fitted SM events	47 ± 6	21 ± 5	8.6 ± 2.8
$t\bar{t}$	22 ± 4	5.9 ± 1.9	1.9 ± 0.7
Single top	9 ± 6	6 ± 5	$2.0^{+2.4}_{-2.0}$
W + jets	11.1 ± 2.9	5.6 ± 1.4	3.7 ± 1.0
Di-/Multiboson	1.23 ± 0.24	0.56 ± 0.11	0.21 ± 0.06
Other	4.8 ± 0.5	2.6 ± 0.4	0.74 ± 0.16
MC exp. SM events	50 ± 7	22 ± 5	8 ± 4
$t\bar{t}$	21 ± 5	4.9 ± 1.6	1.2 ± 0.6
Single top	14 ± 4	9 ± 5	$2.9^{+3.5}_{-2.9}$
W + jets	9.1 ± 1.3	4.5 ± 0.7	3.0 ± 0.6
Di-/Multiboson	1.20 ± 0.23	0.56 ± 0.11	0.21 ± 0.06
Other	4.8 ± 0.5	2.6 ± 0.4	0.74 ± 0.16

signal regions SR-LM, SR-MM and SR-HM, respectively[†]. In the exclusion signal regions, the agreement between data and SM expectation is well within 1σ, except for the SR-LM low m_{CT}, SR-MM medium m_{CT} and SR-HM high m_{CT} bins, where a slight overfluctuation of 1.5σ, 1.6σ and 1.3σ, respectively, is observed in data. Figure 8.4 summarises, across all regions, the observed data, SM background expectation as well as the significances of any observed deviations from the SM expectation.

Since no significant excess is seen in data, the signal regions will be used in the following to derive model-dependent exclusion limits as well as model-independent upper limits on the visible cross section of physics beyond the SM. As a consequence of the minor overfluctuations of data observed in some signal region bins, the observed model-dependent and model-independent limits will be slightly weaker than expected.

[†] The discovery signal regions are not mutually exclusive, thus the small overfluctuations observed in data are not statistically independent in these regions.

Table 8.4: Background-only fit results in the exclusion SRs for an integrated luminosity of 139 fb^{-1}. The first column shows the sum of all m_{CT} bins. Subsequent columns indicate the different bins in m_{CT}, the overflow is included in the last bin. The errors shown include the MC statistical and systematic uncertainties. Uncertainties in the fitted yields are symmetric by construction, except where the negative error is truncated at an event yield of zero. Table adapted from Ref. [185].

SR-LM	All m_{CT} bins	Low m_{CT}	Medium m_{CT}	High m_{CT}
Observed	34	16	11	7
Expected	27 ± 4	8.8 ± 2.8	11.3 ± 3.1	7.3 ± 1.5
$t\bar{t}$	16.2 ± 3.4	4.4 ± 2.2	7.3 ± 2.5	4.6 ± 1.2
Single top	2.7 ± 1.8	1.3 ± 1.1	$0.9^{+1.0}_{-0.9}$	0.6 ± 0.6
W+jets	5.5 ± 2.0	2.0 ± 0.9	2.4 ± 1.3	1.1 ± 0.5
Di-/Multiboson	0.67 ± 0.19	0.39 ± 0.13	$0.09^{+0.11}_{-0.09}$	0.18 ± 0.04
Others	2.23 ± 0.29	0.81 ± 0.25	0.64 ± 0.15	0.77 ± 0.12
SR-MM	All m_{CT} bins	Low m_{CT}	Medium m_{CT}	High m_{CT}
Observed	13	4	7	2
Expected	8.6 ± 2.2	4.6 ± 1.7	2.6 ± 1.3	1.4 ± 0.6
$t\bar{t}$	2.7 ± 1.4	1.6 ± 0.9	0.8 ± 0.7	0.30 ± 0.24
Single top	2.7 ± 1.9	1.6 ± 1.5	$1.0^{+1.1}_{-1.0}$	$0.15^{+0.19}_{-0.15}$
W+jets	1.5 ± 0.7	0.6 ± 0.4	$0.3^{+0.4}_{-0.3}$	0.57 ± 0.26
Di-/Multiboson	0.29 ± 0.08	0.09 ± 0.04	0.065 ± 0.028	0.14 ± 0.06
Others	1.33 ± 0.27	0.69 ± 0.20	0.40 ± 0.13	0.24 ± 0.09
SR-HM	All m_{CT} bins	Low m_{CT}	Medium m_{CT}	High m_{CT}
Observed	14	6	5	3
Expected	8.1 ± 2.7	4.1 ± 1.9	2.9 ± 1.3	1.1 ± 0.5
$t\bar{t}$	1.4 ± 0.5	0.8 ± 0.4	0.36 ± 0.25	0.22 ± 0.15
Single top	$2.0^{+2.4}_{-2.0}$	$0.9^{+1.5}_{-0.9}$	0.9 ± 0.9	$0.16^{+0.26}_{-0.16}$
W+jets	3.7 ± 1.0	1.9 ± 0.8	1.4 ± 0.8	0.45 ± 0.19
Di-/Multiboson	0.21 ± 0.06	0.057 ± 0.025	0.075 ± 0.027	0.08 ± 0.04
Others	0.74 ± 0.16	0.34 ± 0.09	0.19 ± 0.08	0.21 ± 0.08

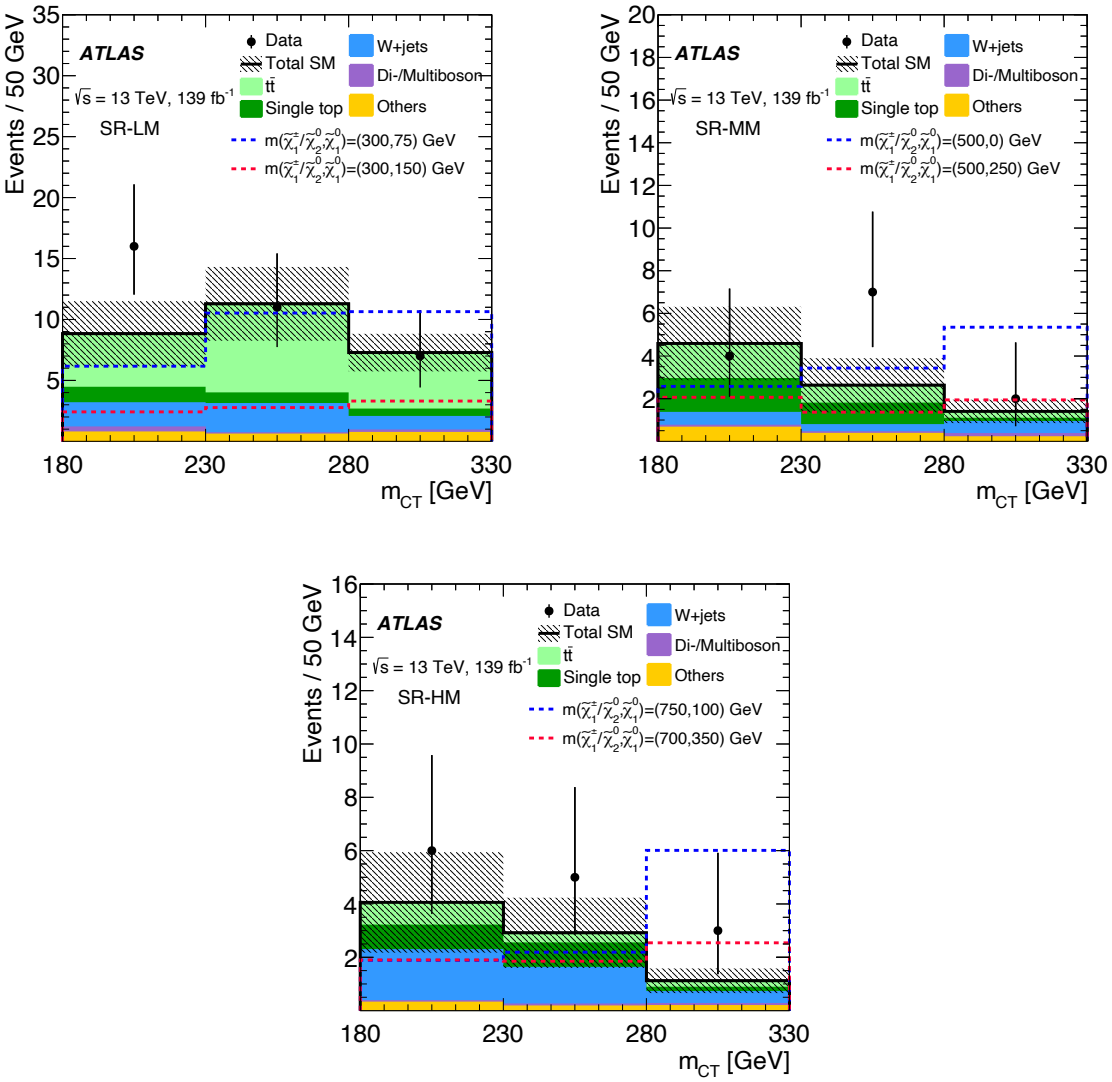

Figure 8.3: Exemplary distribution shown in each exclusion signal region after the background-only fit. The shaded region includes all systematic uncertainties (including correlations) as well as MC statistical uncertainties. Figures adapted from Ref. [185].

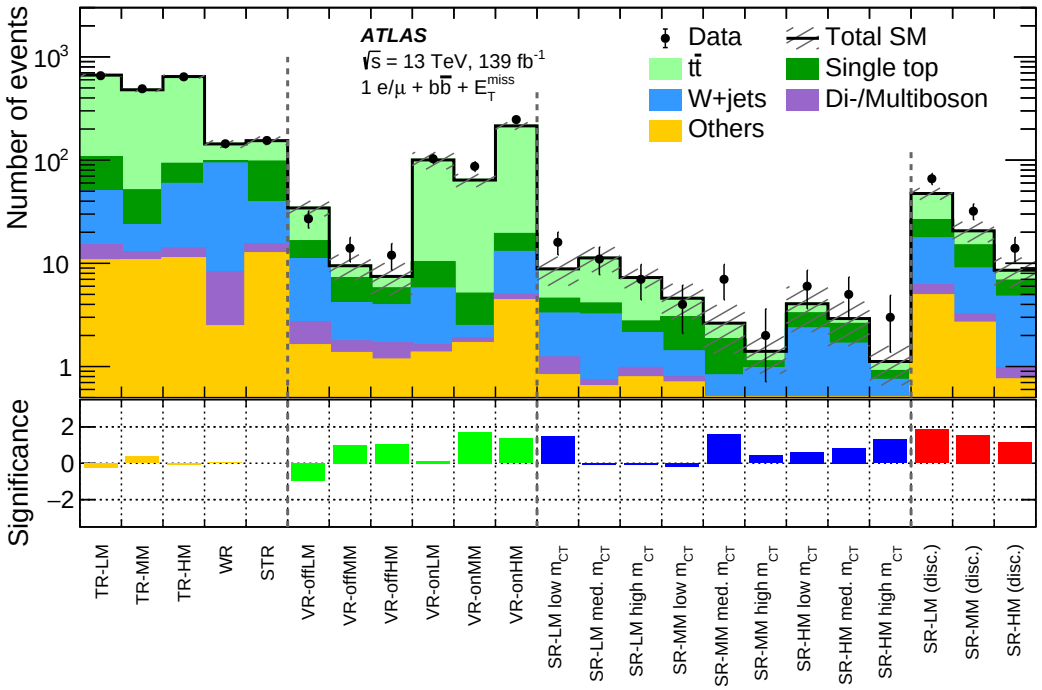

Figure 8.4: Comparison of the observed data and expected event rates in all regions considered in the analysis. The shaded uncertainty band includes both MC statistical and systematic uncertainties. The significances [180] of the differences between the observed data and expected event rates are shown in the bottom panel and discussed in the text. The discovery signal regions are not statistically independent from each other, nor from the exclusion signal regions. Figure adapted from Ref. [185].

8.2 Interpretation

As no significant excess of data is observed in any of the signal regions, model-independent upper limits as well as model-dependent exclusion limits are computed.

8.2.1 Model-independent upper limits

Upper limits on the visible cross section of beyond the Standard Model (BSM) processes, i.e. the product of the cross section of any BSM process and the analysis acceptance times selection efficiency in a given signal region, are derived using the discovery signal regions without any model-dependence. For this, a likelihood containing terms for the control regions and the discovery signal regions is used. Since the discovery signal regions are not statistically independent from each other, only one region enters the likelihood at a time. This results in three distinct fit configurations in which the signal strength μ is the Parameter of Interest (POI) and no signal contamination is assumed in the control regions. The POI is subsequently scanned in distinct steps from zero to high values[†], followed by a hypothesis test at each scan step. The upper limit on the number of observed signal events S^{95}_{obs} is then given by the value of μ for which the corresponding CL_s value drops below 0.05. As reported in table 8.5, observed upper limits on the number of signal events from new physics beyond the SM of 36.8, 24.8 and 14.7 are obtained for the discovery signal regions SR-LM, SR-MM and SR-HM, respectively.

Upper limits on the visible cross section $\langle\epsilon\sigma\rangle^{95}_{\text{obs}}$, are subsequently determined by dividing S^{95}_{obs} by the integrated luminosity of 139 fb^{-1}. For the discovery signal regions SR-LM, SR-MM and SR-HM, observed upper limits on the visible cross section of 0.26 fb, 0.18 fb and 0.11 fb, respectively, are obtained.

In addition to the upper limits on $\langle\epsilon\sigma\rangle^{95}_{\text{obs}}$ and S^{95}_{obs}, table 8.5 also gives the p-values (and corresponding significances) for rejecting the background-only hypothesis in favour of the signal-plus-background hypothesis. As all significances are well below 2σ, the background-only hypothesis cannot be rejected.

8.2.2 Model-dependent exclusion limits

For each signal point in the signal grid considered, a separate model-dependent *exclusion* fit is run using all control regions and exclusion signal regions. As all exclusion signal region bins are mutually exclusive, a likelihood containing terms for all nine signal region bins can be constructed, effectively

[†] The signal strength is in principle allowed to exceed unity in order for the scan to find a 95% CL upper limit

Table 8.5: The 95% CL upper limits on the visible cross-section ($\langle\epsilon\sigma\rangle^{95}_{\text{obs}}$) and on the number of signal events (S^{95}_{obs}) are given. Additionally, the expected 95% CL upper limits on the number of signal events if no BSM signal is present (S^{95}_{exp}) are given, including their $\pm1\sigma$ excursions. The last three columns indicate the confidence level observed for the background-only hypothesis (CL_b), the discovery p-value (p_0) and the significance Z [180].

Signal Region	$\langle\epsilon\sigma\rangle^{95}_{\text{obs}}$[fb]	S^{95}_{obs}	S^{95}_{exp}	CL_b	p_0	Z
SR-LM (disc.)	0.26	36.8	$20.0^{+8.0}_{-5.4}$	0.97	0.03	1.88
SR-MM (disc.)	0.18	24.8	$15.3^{+6.2}_{-4.6}$	0.94	0.06	1.54
SR-HM (disc.)	0.11	14.7	$9.7^{+3.3}_{-2.7}$	0.89	0.10	1.30

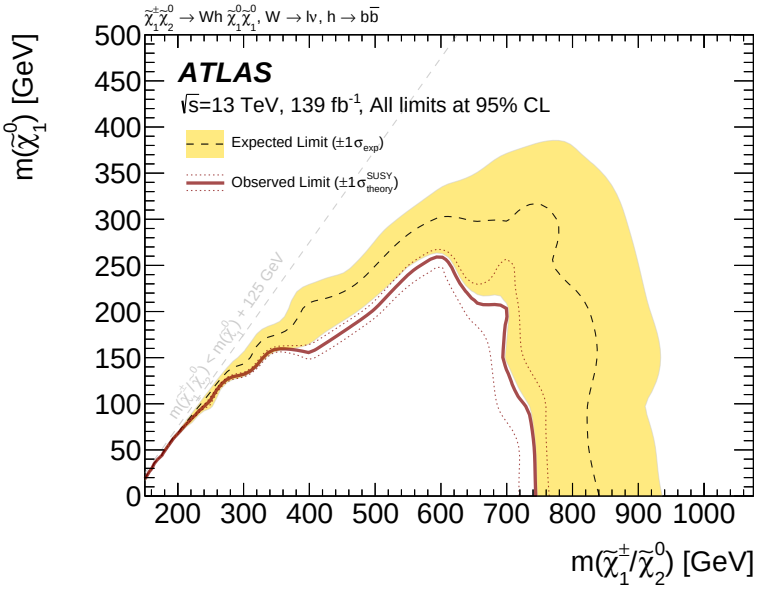

Figure 8.5: Model-dependent exclusion contour on $\tilde{\chi}_1^{\pm}/\tilde{\chi}_2^0$ pair production. The dashed black line represents the expected limit obtained using Asimov data. The uncertainties are given by the yellow band. The red solid line represents the observed limit obtained using 139 fb^{-1} of data taken by ATLAS. By varying the signal cross sections up and down by their uncertainty, the red dashed lines are obtained. All contours are given at 95% CL. Figure adapted from Ref. [185].

creating a shape-fit in the binned variables m_{T} and m_{CT} (cf. chapter 5). As opposed to the background-only fit, the model-dependent exclusion fits allow for signal contribution in all regions. For each point in the signal grid, the expected and observed CL_s values are calculated using the method discussed in section 3.4. Expected (observed) contour lines can then be drawn at expected (observed) $\mathrm{CL}_s = 0.05$ in the $m(\tilde{\chi}_1^{\pm}/\tilde{\chi}_2^0)$–$m(\tilde{\chi}_1^0)$ plane spanned by the simplified model parameters. Signal points inside the contour are excluded at 95% CL. Figure 8.5 shows the exclusion contours obtained in the signal grid considered for the $\tilde{\chi}_1^{\pm}\tilde{\chi}_2^0$ simplified model in the 1ℓ search. The dashed black line corresponds to the expected exclusion contour, obtained using the Asimov dataset. The yellow uncertainty band represents the interval containing 68% of all exclusion contours obtained for repeated observations distributed according to the background-only hypothesis. The solid red line represents the observed exclusion limit obtained using the data recorded by ATLAS. As discussed in section 7.2.2, the dashed red lines are obtained by varying the signal cross sections up and down by 1σ.

Due to the slight overfluctuations of data observed in some of the exclusion signal region bins, the observed limit is slightly weaker than the expected one. The observed exclusion limit extends to about 740 GeV in $m(\tilde{\chi}_1^{\pm}/\tilde{\chi}_2^0)$ for models with a massless $\tilde{\chi}_1^0$, and up to 600 GeV in $m(\tilde{\chi}_1^{\pm}/\tilde{\chi}_2^0)$ for models with $m(\tilde{\chi}_1^0) \simeq 250$ GeV. This extends the previous limit set by ATLAS in this simplified model and decay channel by more than 200 GeV in $m(\tilde{\chi}_1^{\pm}/\tilde{\chi}_2^0)$ for a light $\tilde{\chi}_1^0$, an improvement made possible not only by the significant increase in integrated luminosity but also by the introduction of a two-dimensional shape fit in the analysis strategy (cf. fig. 5.4(b)).

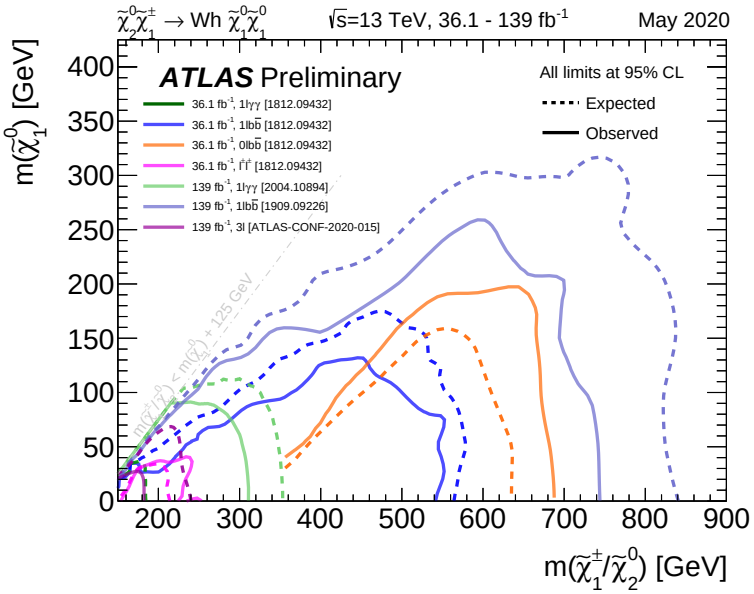

Figure 8.6: Summary of ATLAS limits on $m(\tilde{\chi}_1^\pm/\tilde{\chi}_2^0)$ masses in the $\tilde{\chi}_1^\pm\tilde{\chi}_2^0 \rightarrow Wh\tilde{\chi}_1^0\tilde{\chi}_1^0$ simplified model. The exclusion limit obtained by the analysis presented in this work is referred to as *1Lbb* (the 139 fb^{-1} iteration, drawn in light blue) and is the most stringent limit in this simplified model set by an ATLAS search thus far. Figure adapted from Ref. [258].

8.3 Discussion

At the time of writing, the limits derived in this analysis are the most stringent limits on the $\tilde{\chi}_1^\pm\tilde{\chi}_2^0 \rightarrow Wh\tilde{\chi}_1^0\tilde{\chi}_1^0$ simplified model set by an ATLAS search, surpassing not only the previous iteration of the analysis [183], but also yielding more stringent limits than those published by ATLAS in other decay channels of the same simplified model [258]. Figure 8.6 shows a summary of results published by ATLAS searches in the $\tilde{\chi}_1^\pm\tilde{\chi}_2^0 \rightarrow Wh\tilde{\chi}_1^0\tilde{\chi}_1^0$ simplified model. Recently, a CMS search for Supersymmetry (SUSY), interpreted using the same simplified model and targeting the 1ℓ final state has excluded $m(\tilde{\chi}_1^\pm/\tilde{\chi}_2^0)$ masses up to 820 GeV for a massless lightest supersymmetric particle (LSP) [259].

Various other searches for SUSY at both ATLAS and CMS are constraining a multitude of supersymmetric particle production and decay processes. The limits on gluino and squark pair production at the Large Hadron Collider (LHC) are particularly heavily constrained, reaching 2 TeV in many cases. With the large integrated luminosity available through the full Run 2 dataset, and the improved analysis techniques and strategies developed over the last years, the typically weaker limits on electroweakinos and sleptons are also significantly increasing and, in some cases, approach the 1 TeV mark (cf. fig. A.11 and Refs. [258, 260]). The diverse SUSY search programs at ATLAS and CMS thus increasingly constrain the existence of SUSY at the TeV scale at the LHC. Still, a number of arguments can be made that discarding the possibility for SUSY to exist at the energies available with the LHC is much too early. By the end of the lifetime of the LHC, including the High Luminosity LHC (HL-LHC), a projected amount of 3000 fb^{-1} [261] will have been delivered to the particle physics experiments. Many supersymmetric models not accessible with the full Run 2 dataset using today's analyses will hence only come into reach in the upcoming runs of the LHC.

More importantly, however, most of the quoted limits assume simplified models and are thus only valid if the assumptions of the respective simplified model are satisfied. In any realistic supersymmetric scenario that might be realised in nature and that is accessible to the LHC, assumptions like 100% branching fractions or a small set of supersymmetric particles participating in the decay chains are likely not exactly fulfilled. Thus, the quoted simplified model limits can in general not be trivially interpreted as the true underlying constraint on the respective parameter of a more realistic supersymmetric scenario. Due to the optimistic assumptions like 100% branching fractions, the true constraints will in general be weaker than the simplified model limits. Reinterpretations of Run 1 ATLAS searches for SUSY in the phenomenological Minimal Supersymmetric Standard Model (pMSSM) [87] have indeed shown that, in more complex SUSY models, constraints on the masses of supersymmetric particles are somewhat weaker than those quoted for the simplified models studied in the respective analyses.

Naturally, there is a large interest in the high energy physics (HEP) community to perform reinterpretations of the existing searches for SUSY in additional, promising signal models. Compelling reasons for performing reinterpretations within the ATLAS Collaboration include, amongst others, the possibility to state a combined sensitivity of the ATLAS SUSY search programme to more realistic and complex SUSY scenarios (compared to the simplified model limits). Such models are, however, embedded in high-dimensional parameter spaces and depend on a large set of parameters, meaning reinterpretations are computationally extremely expensive or even unfeasible. In order to perform large-scale reinterpretations in model spaces like the pMSSM, appropriate analysis approximations are necessary. For this reason, the next part of this thesis will introduce and discuss analysis approximations and apply them in a reinterpretation of the 1ℓ search in the pMSSM.

Part III

Reinterpretation

Part IV

Summary and Outlook

Part V

Appendices

Appendix A

Additional analysis material

This appendix provides additional analysis material for the 1ℓ search presented in part II of this thesis.

A.1 Kinematic distributions

Figure A.1 illustrates the dependence of the distributions of relevant kinematic observables on the electroweakino mass scale and the mass difference between $\tilde{\chi}_1^\pm/\tilde{\chi}_2^0$ and $\tilde{\chi}_1^0$. In the plots on the left column of fig. A.1, only $m(\tilde{\chi}_1^\pm/\tilde{\chi}_2^0)$ is varied while $m(\tilde{\chi}_1^0)$ is kept to be massless. On the right-hand side of fig. A.1, $m(\tilde{\chi}_1^\pm/\tilde{\chi}_2^0)$ is fixed at 450 GeV, while $m(\tilde{\chi}_1^0)$ is varied. As can be observed, model points with increasing $\tilde{\chi}_1^\pm/\tilde{\chi}_2^0$ mass show increasing values in kinematic observables like $E_\mathrm{T}^\mathrm{miss}$, m_T, m_CT and the p_T of the lepton. Model points with increasingly small electroweakino mass differences tend to exhibit less $E_\mathrm{T}^\mathrm{miss}$ and overall softer objects (as e.g. more events with leptons with relatively low p_T).

A.2 Signal region optimisation

A.2.1 Raw results from *N*-dimensional scan

Figure A.2 shows the results of the N-dimensional cut scan for all benchmark signal points considered. As in chapter 5, three different uncertainty configurations are used for computing the significance Z_B, and all values are computed for the two statistically independent subsets of the MC datasets used during the N-dimensional scan. This approach allows to gauge the impact of statistical fluctuations on the cut combinations tested.

By choosing a well-performing cut combination for each benchmark point, the optimised selections in figs. A.3 to A.8 are found after a round of $N-1$ plots. As discussed in section 5.2.2 the optimal cut combinations for each benchmark signal point are consolidated into multiple signal regions designed to be sensitive to different kinematic regions of the model parameter space.

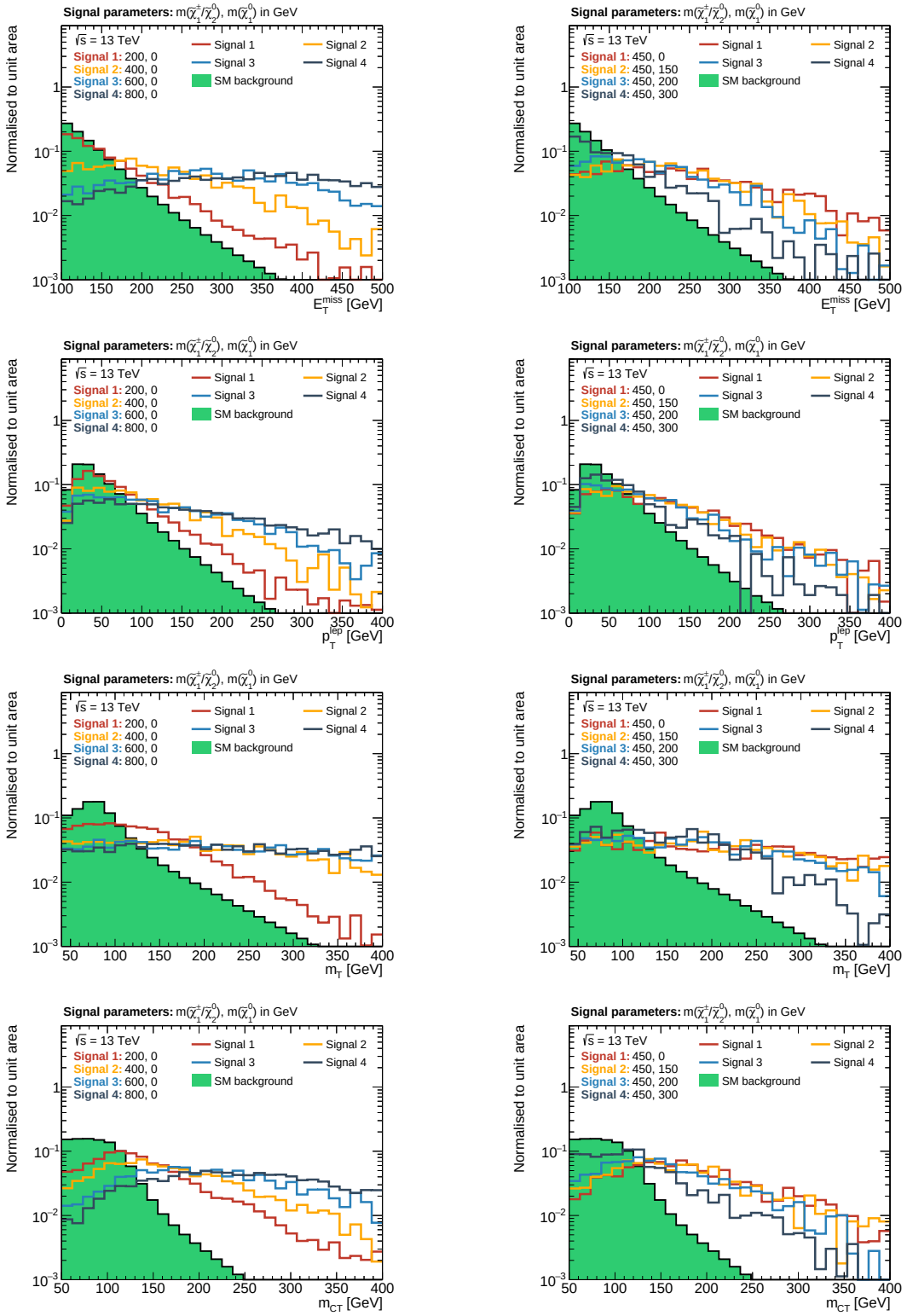

Figure A.1: Dependence of some of the kinematic observables on the $\tilde{\chi}_1^\pm/\tilde{\chi}_2^0$ mass scale (left) and $\tilde{\chi}_1^\pm/\tilde{\chi}_2^0-\tilde{\chi}_1^0$ mass differences (right). The simulated SM backgrounds are stacked on top of each other and summarised in a single 'SM' histogram. Distributions from exemplary signal models with the quoted mass parameters are overlaid. In order to emphasise the shape differences, both total background and signal distributions are normalised to unity. A preselection requiring a lepton, at least two jets and $E_{\mathrm{T}}^{\mathrm{miss}} > 100\,\mathrm{GeV}$ is applied.

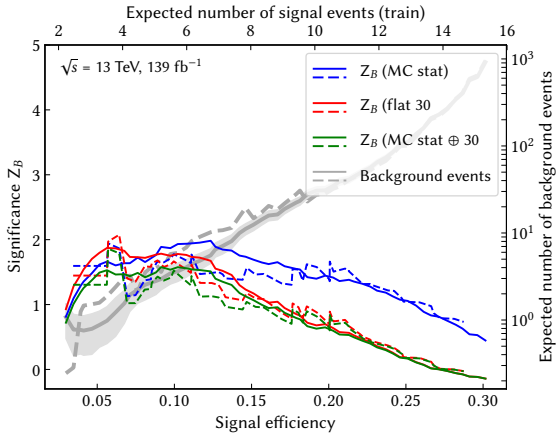

(a) $m(\tilde{\chi}_1^\pm/\tilde{\chi}_2^0), m(\tilde{\chi}_1^0) = 800, 250$ GeV

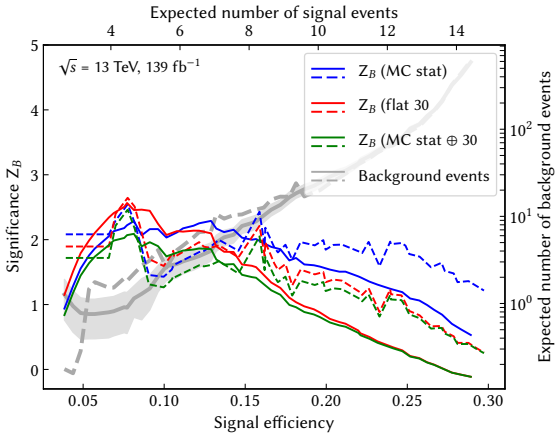

(b) $m(\tilde{\chi}_1^\pm/\tilde{\chi}_2^0), m(\tilde{\chi}_1^0) = 800, 150$ GeV

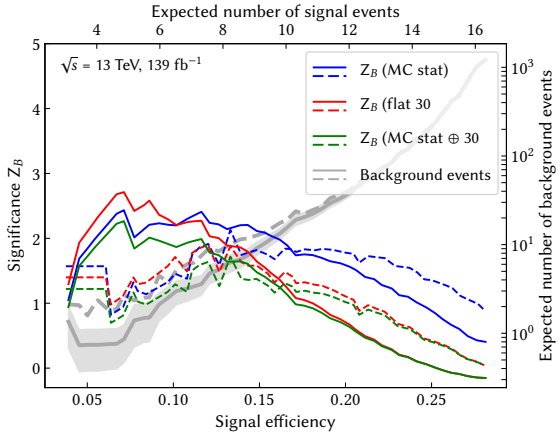

(c) $m(\tilde{\chi}_1^\pm/\tilde{\chi}_2^0), m(\tilde{\chi}_1^0) = 800, 0$ GeV

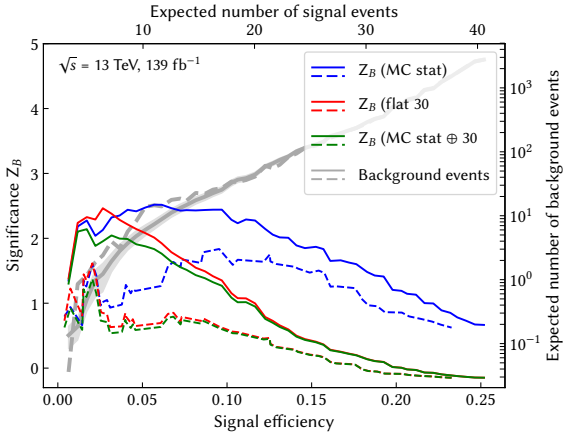

(d) $m(\tilde{\chi}_1^\pm/\tilde{\chi}_2^0), m(\tilde{\chi}_1^0) = 600, 300$ GeV

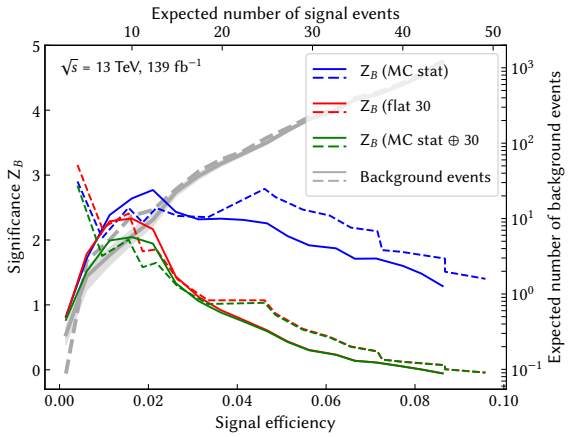

(e) $m(\tilde{\chi}_1^\pm/\tilde{\chi}_2^0), m(\tilde{\chi}_1^0) = 400, 200$ GeV

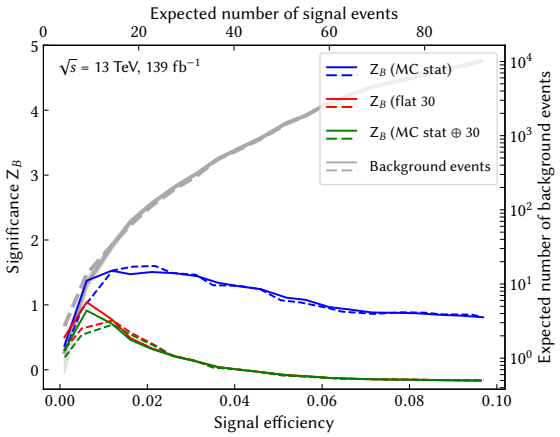

(f) $m(\tilde{\chi}_1^\pm/\tilde{\chi}_2^0), m(\tilde{\chi}_1^0) = 300, 150$ GeV

Figure A.2: Results of the N-dimensional cut scan for all benchmark points. The binomial discovery significance Z_B is plotted against the signal efficiency for varying uncertainty configurations. Additionally, the expected SM background rates are shown, including statistical uncertainties for one of the two statistically independent samples (shaded area). The solid and dashed lines represent the two statistically independent subsets that the MC datasets are split into.

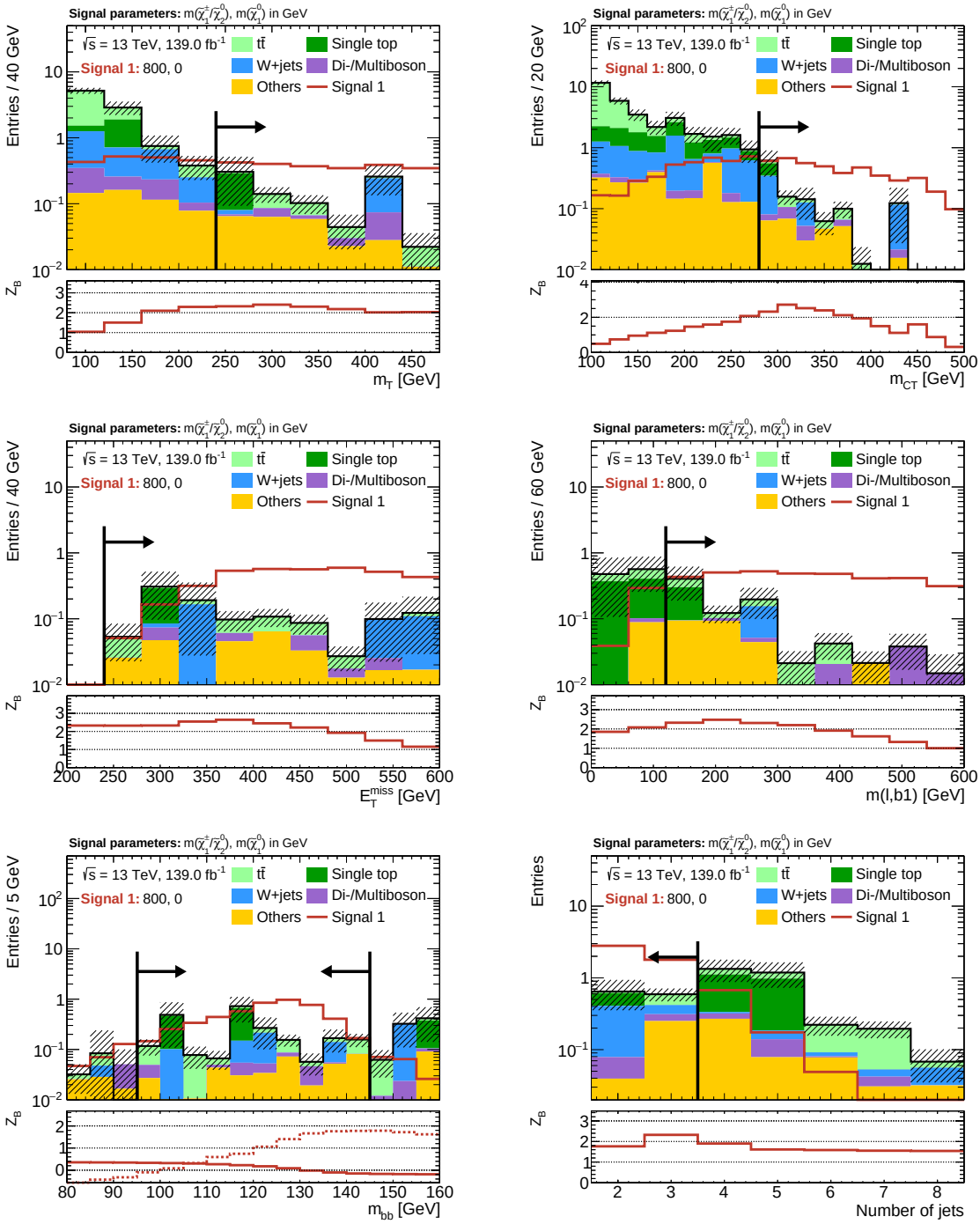

Figure A.3: $N-1$ plots for the chosen cut combination for the $(m(\tilde{\chi}_1^\pm/\tilde{\chi}_2^0), m(\tilde{\chi}_1^0)) = (800\,\text{GeV}, 0\,\text{GeV})$ signal point. The shaded region includes MC statistical as well as 30% systematic uncertainties (added in quadrature) on the background. The significance is computed using the binomial discovery significance using the uncertainty on the background.

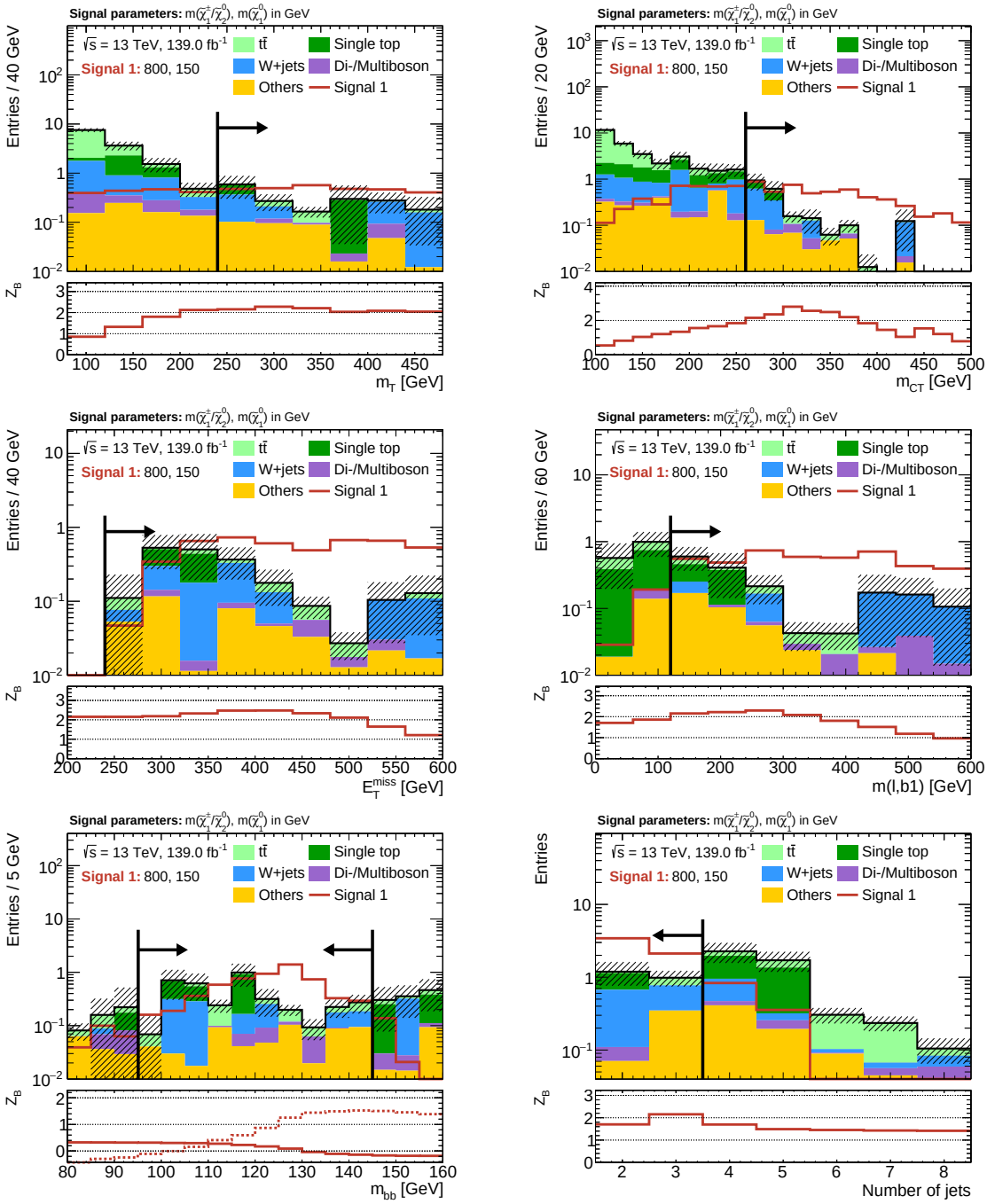

Figure A.4: N-1 plots for the chosen cut combination for the $(m(\tilde{\chi}_1^\pm/\tilde{\chi}_2^0), m(\tilde{\chi}_1^0)) = (800\,\text{GeV}, 150\,\text{GeV})$ signal point. The shaded region includes MC statistical as well as 30% systematic uncertainties (added in quadrature) on the background. The significance is computed using the binomial discovery significance using the uncertainty on the background.

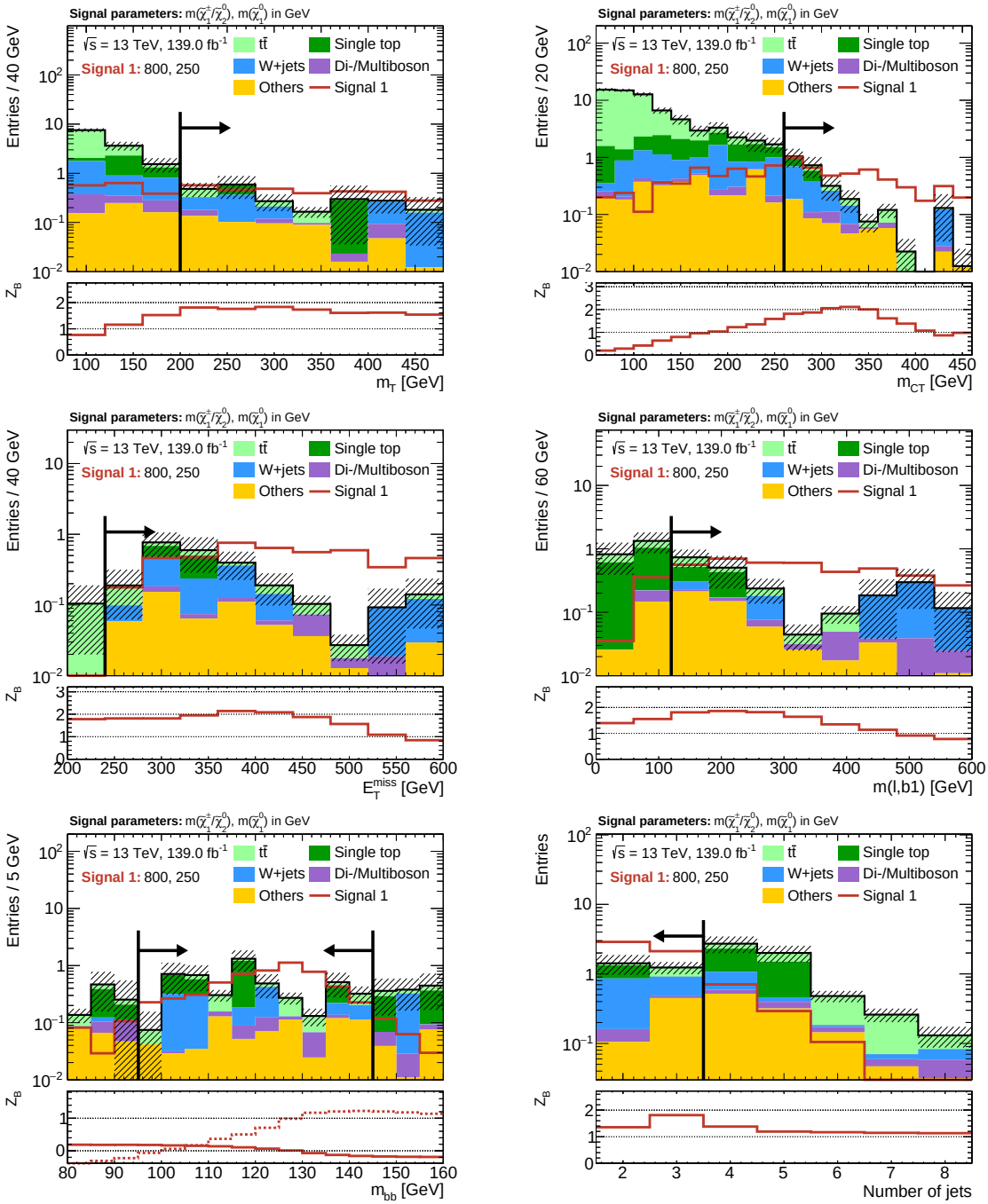

Figure A.5: $N-1$ plots for the chosen cut combination for the $(m(\tilde{\chi}_1^\pm/\tilde{\chi}_2^0), m(\tilde{\chi}_1^0)) = (800\,\text{GeV}, 250\,\text{GeV})$ signal point. The shaded region includes MC statistical as well as 30% systematic uncertainties (added in quadrature) on the background. The significance is computed using the binomial discovery significance using the uncertainty on the background.

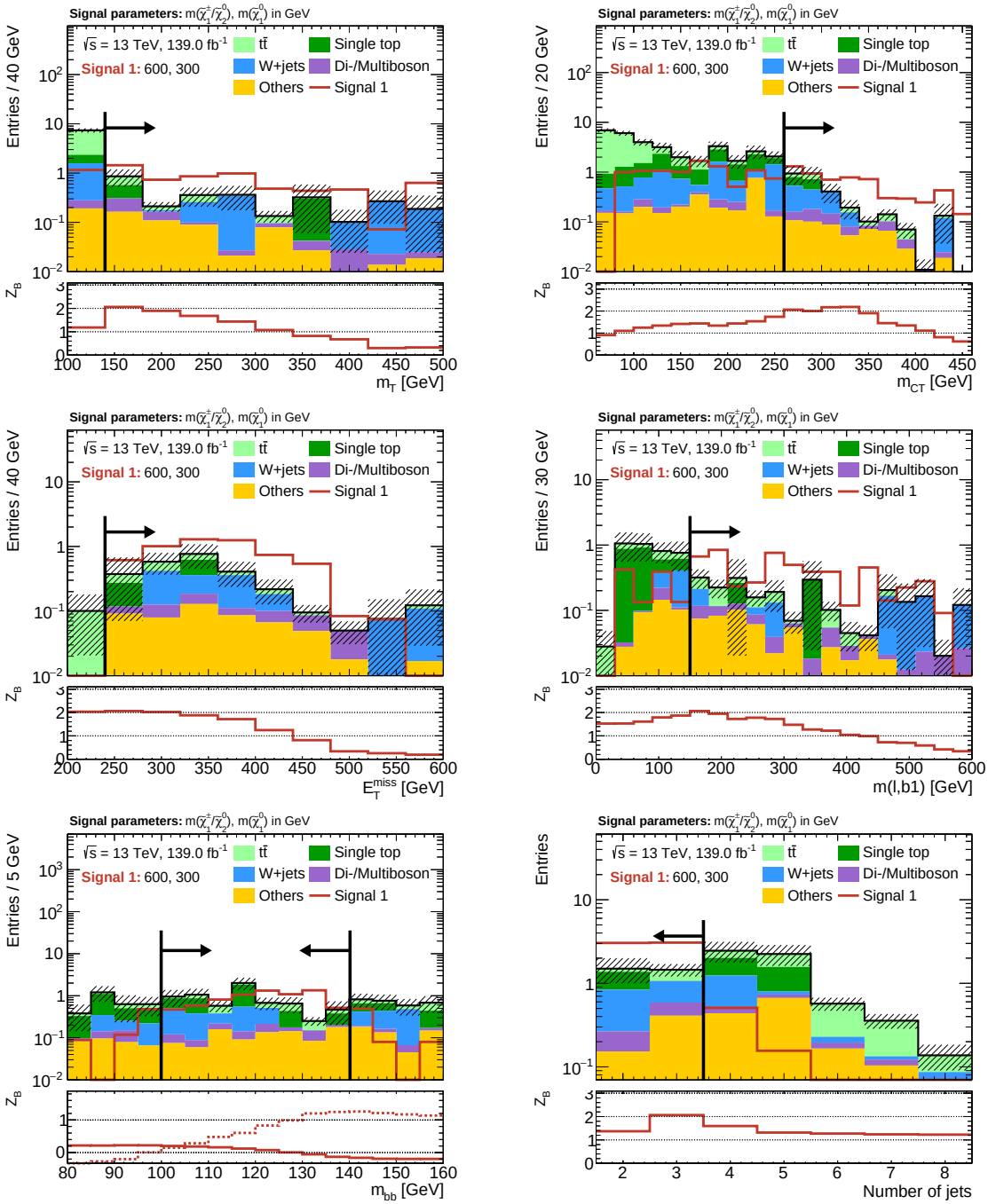

Figure A.6: $N-1$ plots for the chosen cut combination for the $(m(\tilde{\chi}_1^\pm/\tilde{\chi}_2^0), m(\tilde{\chi}_1^0)) = (600\,\text{GeV}, 300\,\text{GeV})$ signal point. The shaded region includes MC statistical as well as 30% systematic uncertainties (added in quadrature) on the background. The significance is computed using the binomial discovery significance using the uncertainty on the background.

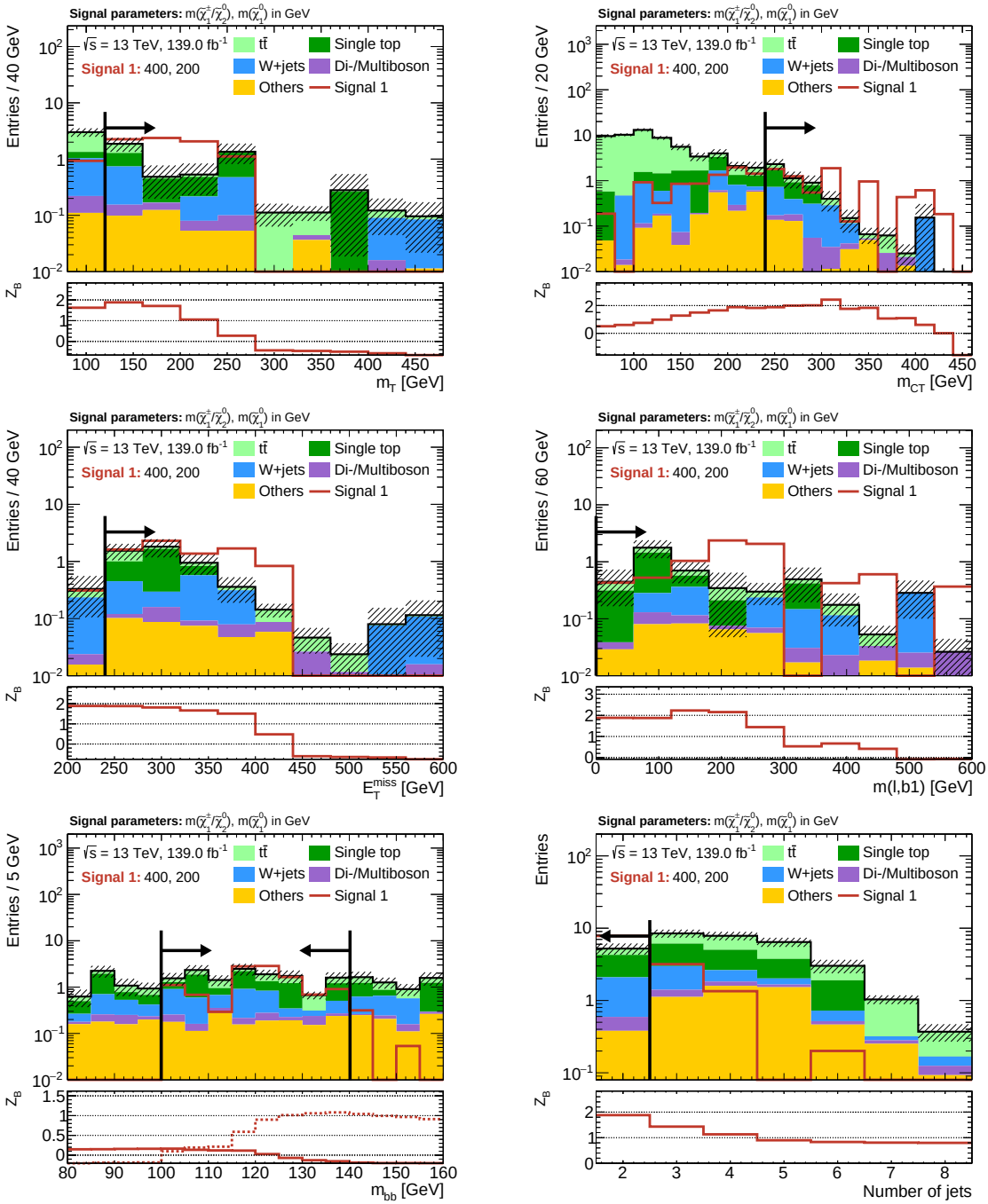

Figure A.7: N-1 plots for the chosen cut combination for the $(m(\tilde{\chi}_1^\pm/\tilde{\chi}_2^0), m(\tilde{\chi}_1^0)) = (400\,\text{GeV}, 200\,\text{GeV})$ signal point. The shaded region includes MC statistical as well as 30% systematic uncertainties (added in quadrature) on the background. The significance is computed using the binomial discovery significance using the uncertainty on the background.

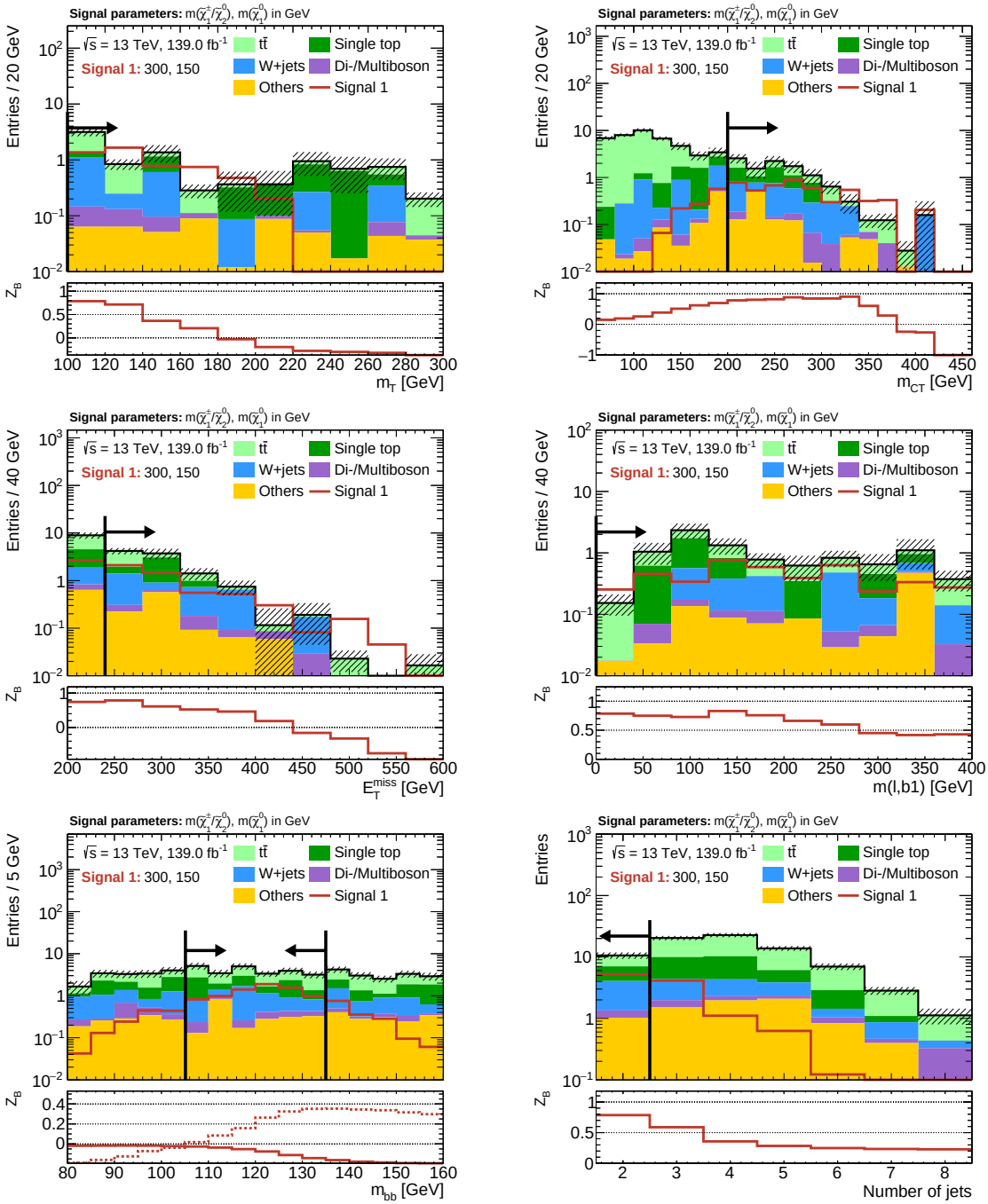

Figure A.8: $N-1$ plots for the chosen cut combination for the $(m(\tilde{\chi}_1^\pm/\tilde{\chi}_2^0), m(\tilde{\chi}_1^0)) = (300\,\text{GeV}, 150\,\text{GeV})$ signal point. The shaded region includes MC statistical as well as 30% systematic uncertainties (added in quadrature) on the background. The significance is computed using the binomial discovery significance using the uncertainty on the background.

A.2.2 Impact of $m_{\ell b_1}$

As discussed in section 4.6, the distribution of $m_{\ell b_1}$ has a kinematic endpoint at about 153 GeV for $t\bar{t}$ and single top production events where the lepton and leading b-jet originate from the same top quark decay. In the SUSY processes considered, $m_{\ell b_1}$ depends on the mass-scale of the electroweakinos pair-produced, and thus offers especially good discriminative power in the high electroweakino mass regime targeted by SR-HM.

Figure A.9 illustrates the impact of adding a requirement of $m_{\ell b_1} > 120$ GeV in SR-HM, revealing a noticeable increase in sensitivity towards high electroweakino masses. Studies have shown that the addition of $m_{\ell b_1} > 120$ GeV to the remaining signal regions does not improve the sensitivity further.

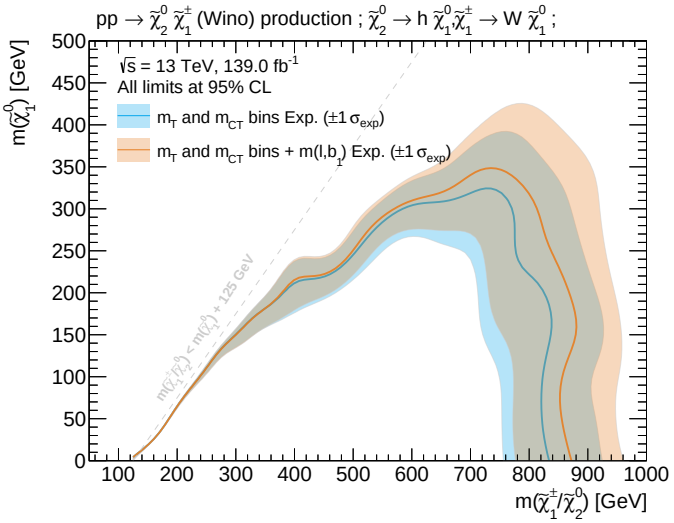

Figure A.9: Comparison of different shape-fit configurations, illustrating the sensitivity increase achieved through a requirement on high $m_{\ell b_1}$ values in SR-HM on top of the two-dimensional shape-fit in m_{T} and m_{CT}. All exclusion limits shown are expected limits at 95% CL, using MC statistical and 30% systematic uncertainties. Background estimation in the signal regions is taken directly from MC for all SM backgrounds.

A.3 Background estimation

The signal contamination in all validation regions is shown in fig. A.10. In the VR-off regions the maximum signal contamination is found to be about 7%–13%, depending on the requirement on m_{T}. In the VR-on regions, the maximum signal contamination amounts to about 5%–14%, depending again on the m_{T}-bin.

A.4 Summary of results of ATLAS searches for SUSY

Figure A.11 provides a comprehensive summary of current results of ATLAS searches for SUSY. The limits on the sparticle masses set by different searches in various models and signatures are given.

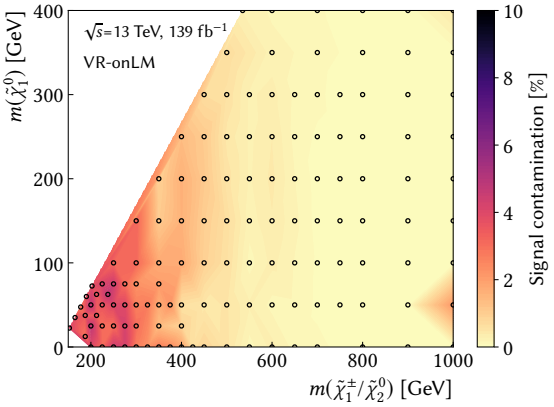

(a) VR-onLM

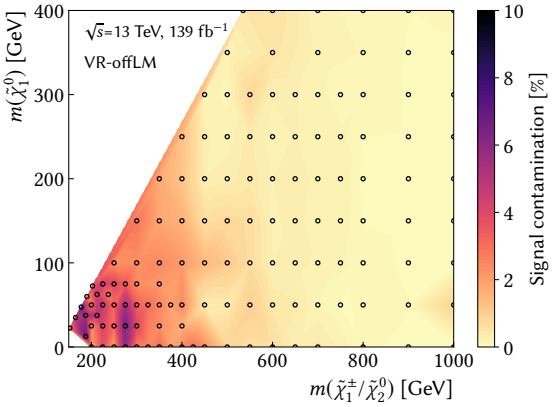

(b) VR-offLM

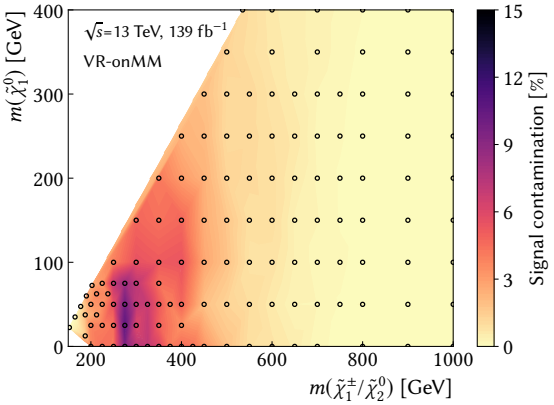

(c) VR-onMM

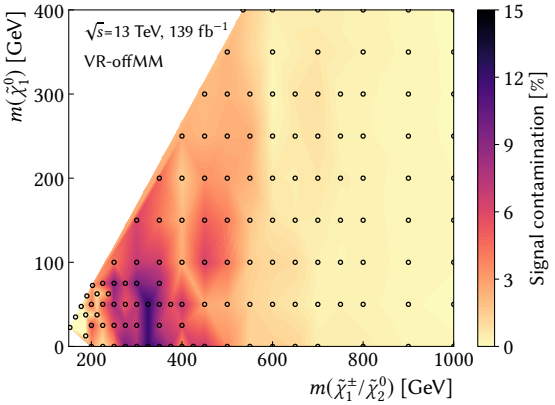

(d) VR-offMM

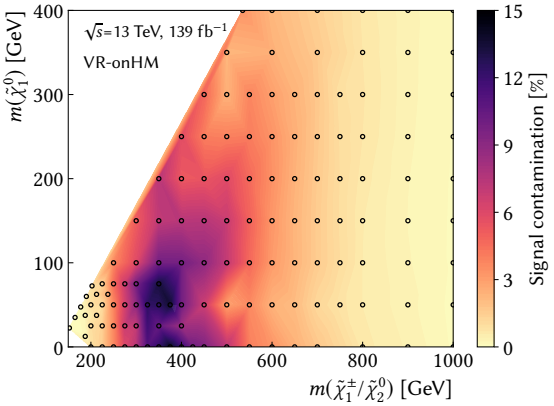

(e) VR-onHM

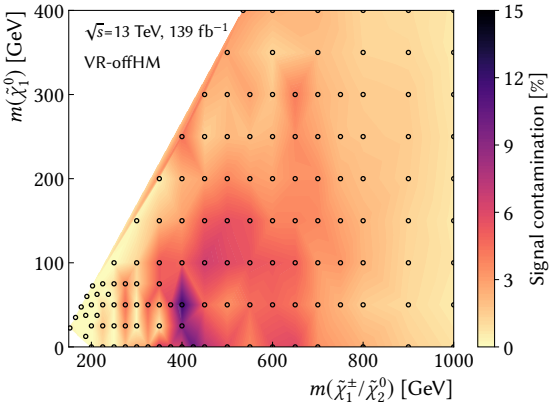

(f) VR-offHM

Figure A.10: Signal contamination (shown on the *z-axis*) for all VRs throughout the signal grid. The space between the signal points (indicated by the black circles) is interpolated using Delaunay triangles.

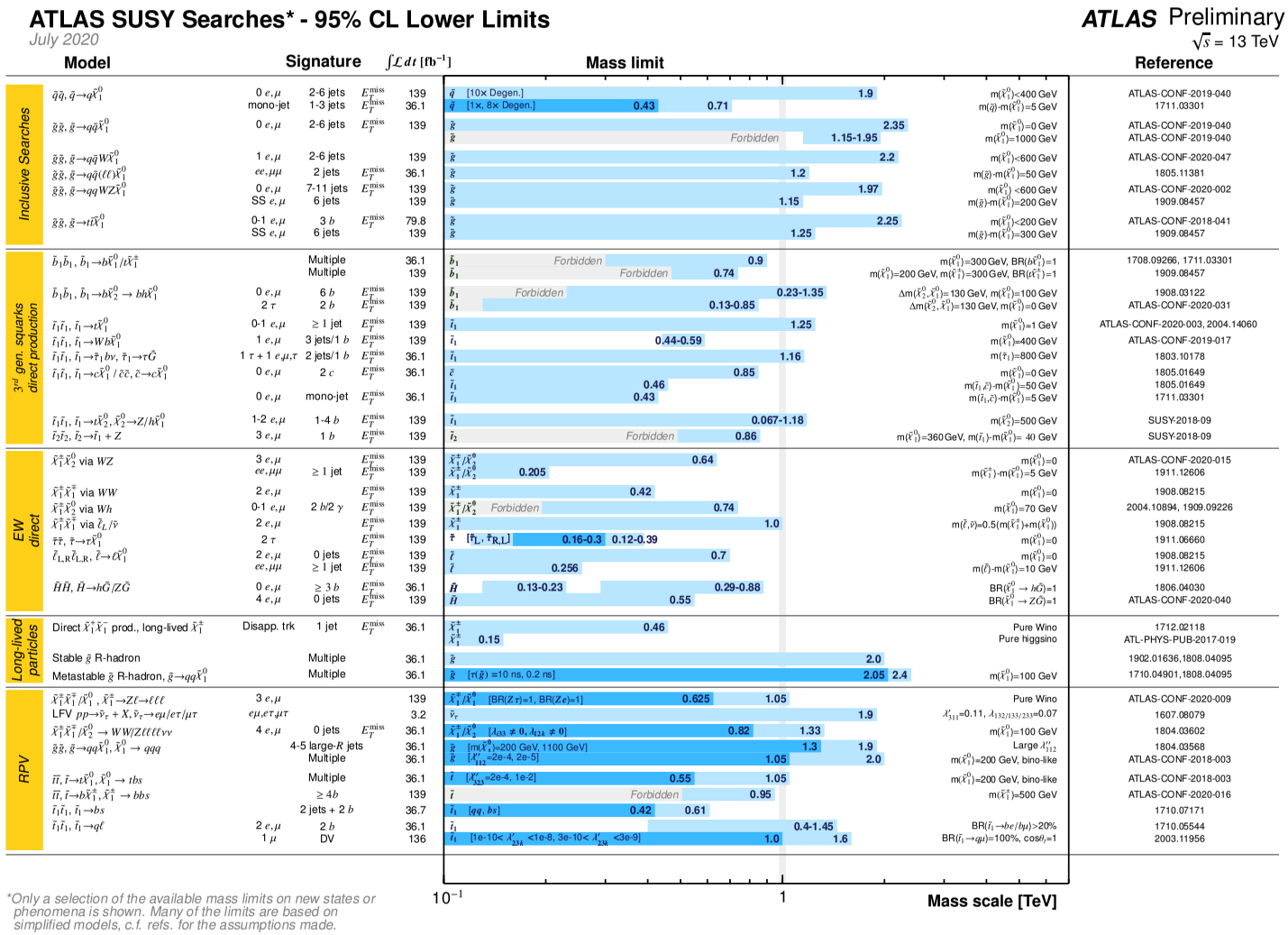

Figure A.11: Summary of the results of ATLAS searches for SUSY. A representative selection of the available search results is shown. Results are given with respect to the nominal cross section. In some cases additional dependencies are indicated by darker bands showing different model parameters. Figure adapted from Ref. [258].

Abbreviations

BSM beyond the Standard Model. 124

CR control region. 115–117, 119

HEP high energy physics. 127

HL-LHC High Luminosity LHC. 126

LHC Large Hadron Collider. 126, 127

LSP lightest supersymmetric particle. 126

MC Monte Carlo. 115–123, 179, 181–188

pMSSM phenomenological Minimal Supersymmetric Standard Model. 127

POI Parameter of Interest. 124

SM Standard Model. 115, 117, 119, 120, 124, 180, 181, 188

SR signal region. 117, 119–121

SUSY Supersymmetry. 126, 127, 188–190

VR validation region. 117–119, 189

Bibliography

[1] ATLAS Collaboration, "Observation of a new particle in the search for the Standard Model Higgs boson with the ATLAS detector at the LHC," *Phys. Lett. B* **716** (2012) 1, arXiv:1207.7214 [hep-ex].

[2] CMS Collaboration, "Observation of a new boson at a mass of 125 GeV with the CMS experiment at the LHC," *Phys. Lett. B* **716** (2012) 30, arXiv:1207.7235 [hep-ex].

[3] I. C. Brock and T. Schorner-Sadenius, *Physics at the terascale*. Wiley, Weinheim, 2011. https://cds.cern.ch/record/1354959.

[4] M. E. Peskin and D. V. Schroeder, *An Introduction to quantum field theory*. Addison-Wesley, Reading, USA, 1995. http://www.slac.stanford.edu/~mpeskin/QFT.html.

[5] S. P. Martin, "A Supersymmetry primer," arXiv:hep-ph/9709356v7 [hep-ph]. [Adv. Ser. Direct. High Energy Phys.18,1(1998)].

[6] M. Bustamante, L. Cieri, and J. Ellis, "Beyond the Standard Model for Montaneros," in *5th CERN - Latin American School of High-Energy Physics*. 11, 2009. arXiv:0911.4409 [hep-ph].

[7] L. Brown, *The Birth of particle physics*. Cambridge University Press, Cambridge Cambridgeshire New York, 1986.

[8] P. J. Mohr, D. B. Newell, and B. N. Taylor, "CODATA Recommended Values of the Fundamental Physical Constants: 2014," *Rev. Mod. Phys.* **88** no. 3, (2016) 035009, arXiv:1507.07956 [physics.atom-ph].

[9] Particle Data Group, "Review of Particle Physics," *Progress of Theoretical and Experimental Physics* **2020** no. 8, (08, 2020) , https://academic.oup.com/ptep/article-pdf/2020/8/083C01/34673722/ptaa104.pdf. https://doi.org/10.1093/ptep/ptaa104. 083C01.

[10] Super-Kamiokande Collaboration, "Evidence for oscillation of atmospheric neutrinos," *Phys. Rev. Lett.* **81** (1998) 1562–1567, arXiv:hep-ex/9807003 [hep-ex].

[11] Z. Maki, M. Nakagawa, and S. Sakata, "Remarks on the unified model of elementary particles," *Prog. Theor. Phys.* **28** (1962) 870–880. [,34(1962)].

[12] N. Cabibbo, "Unitary symmetry and leptonic decays," *Phys. Rev. Lett.* **10** (Jun, 1963) 531–533. https://link.aps.org/doi/10.1103/PhysRevLett.10.531.

[13] M. Kobayashi and T. Maskawa, "CP Violation in the Renormalizable Theory of Weak Interaction," *Prog. Theor. Phys.* **49** (1973) 652–657.

[14] E. Noether and M. A. Tavel, "Invariant variation problems," arXiv:physics/0503066.

[15] J. C. Ward, "An identity in quantum electrodynamics," *Phys. Rev.* **78** (Apr, 1950) 182–182. https://link.aps.org/doi/10.1103/PhysRev.78.182.

[16] Y. Takahashi, "On the generalized ward identity," *Il Nuovo Cimento (1955-1965)* **6** no. 2, (Aug, 1957) 371–375. https://doi.org/10.1007/BF02832514.

[17] G. 'tHooft, "Renormalization of massless yang-mills fields," *Nuclear Physics B* **33** no. 1, (1971) 173 – 199. http://www.sciencedirect.com/science/article/pii/0550321371903956.

[18] J. Taylor, "Ward identities and charge renormalization of the yang-mills field," *Nuclear Physics B* **33** no. 2, (1971) 436 – 444. http://www.sciencedirect.com/science/article/pii/0550321371902975.

[19] A. A. Slavnov, "Ward identities in gauge theories," *Theoretical and Mathematical Physics* **10** no. 2, (Feb, 1972) 99–104. https://doi.org/10.1007/BF01090719.

[20] C. N. Yang and R. L. Mills, "Conservation of isotopic spin and isotopic gauge invariance," *Phys. Rev.* **96** (Oct, 1954) 191–195. https://link.aps.org/doi/10.1103/PhysRev.96.191.

[21] K. G. Wilson, "Confinement of quarks," *Phys. Rev. D* **10** (Oct, 1974) 2445–2459. https://link.aps.org/doi/10.1103/PhysRevD.10.2445.

[22] T. DeGrand and C. DeTar, *Lattice Methods for Quantum Chromodynamics*. World Scientific, Singapore, 2006. https://cds.cern.ch/record/1055545.

[23] S. L. Glashow, "Partial-symmetries of weak interactions," *Nuclear Physics* **22** no. 4, (1961) 579 – 588. http://www.sciencedirect.com/science/article/pii/0029558261904692.

[24] S. Weinberg, "A model of leptons," *Phys. Rev. Lett.* **19** (Nov, 1967) 1264–1266. https://link.aps.org/doi/10.1103/PhysRevLett.19.1264.

[25] A. Salam and J. C. Ward, "Weak and electromagnetic interactions," *Il Nuovo Cimento (1955-1965)* **11** no. 4, (Feb, 1959) 568–577. https://doi.org/10.1007/BF02726525.

[26] C. S. Wu, E. Ambler, R. W. Hayward, *et al.*, "Experimental test of parity conservation in beta decay," *Phys. Rev.* **105** (Feb, 1957) 1413–1415. https://link.aps.org/doi/10.1103/PhysRev.105.1413.

[27] M. Gell-Mann, "The interpretation of the new particles as displaced charge multiplets," *Il Nuovo Cimento (1955-1965)* **4** no. 2, (Apr, 1956) 848–866. https://doi.org/10.1007/BF02748000.

[28] K. Nishijima, "Charge Independence Theory of V Particles*," *Progress of Theoretical Physics* **13** no. 3, (03, 1955) 285–304, https://academic.oup.com/ptp/article-pdf/13/3/285/5425869/13-3-285.pdf. https://doi.org/10.1143/PTP.13.285.

[29] T. Nakano and K. Nishijima, "Charge Independence for V-particles*," *Progress of Theoretical Physics* **10** no. 5, (11, 1953) 581–582, https://academic.oup.com/ptp/article-pdf/10/5/581/5364926/10-5-581.pdf. https://doi.org/10.1143/PTP.10.581.

[30] F. Englert and R. Brout, "Broken symmetry and the mass of gauge vector mesons," *Phys. Rev. Lett.* **13** (Aug, 1964) 321–323. https://link.aps.org/doi/10.1103/PhysRevLett.13.321.

[31] P. W. Higgs, "Broken symmetries and the masses of gauge bosons," *Phys. Rev. Lett.* **13** (Oct, 1964) 508–509. https://link.aps.org/doi/10.1103/PhysRevLett.13.508.

[32] P. W. Higgs, "Spontaneous symmetry breakdown without massless bosons," *Phys. Rev.* **145** (May, 1966) 1156–1163. https://link.aps.org/doi/10.1103/PhysRev.145.1156.

[33] Y. Nambu, "Quasiparticles and Gauge Invariance in the Theory of Superconductivity," *Phys. Rev.* **117** (1960) 648–663. [,132(1960)].

[34] J. Goldstone, "Field Theories with Superconductor Solutions," *Nuovo Cim.* **19** (1961) 154–164.

[35] V. Brdar, A. J. Helmboldt, S. Iwamoto, and K. Schmitz, "Type-I Seesaw as the Common Origin of Neutrino Mass, Baryon Asymmetry, and the Electroweak Scale," *Phys. Rev. D* **100** (2019) 075029, arXiv:1905.12634 [hep-ph].

[36] G. 't Hooft and M. Veltman, "Regularization and renormalization of gauge fields," *Nuclear Physics B* **44** no. 1, (1972) 189 – 213. http://www.sciencedirect.com/science/article/pii/0550321372902799.

[37] G. L. Kane, *The supersymmetric world : the beginnings of the theory.* World Scientific, Singapore River Edge, N.J, 2000.

[38] F. Zwicky, "Die Rotverschiebung von extragalaktischen Nebeln," *Helv. Phys. Acta* **6** (1933) 110–127. https://cds.cern.ch/record/437297.

[39] V. C. Rubin and W. K. Ford, Jr., "Rotation of the Andromeda Nebula from a Spectroscopic Survey of Emission Regions," *Astrophys. J.* **159** (1970) 379–403.

[40] G. Bertone, D. Hooper, and J. Silk, "Particle dark matter: Evidence, candidates and constraints," *Phys. Rept.* **405** (2005) 279–390, arXiv:hep-ph/0404175.

[41] D. Clowe, M. Bradac, A. H. Gonzalez, *et al.*, "A direct empirical proof of the existence of dark matter," *Astrophys. J.* **648** (2006) L109–L113, arXiv:astro-ph/0608407 [astro-ph].

[42] A. Taylor, S. Dye, T. J. Broadhurst, *et al.*, "Gravitational lens magnification and the mass of abell 1689," *Astrophys. J.* **501** (1998) 539, arXiv:astro-ph/9801158.

[43] C. Bennett *et al.*, "Four year COBE DMR cosmic microwave background observations: Maps and basic results," *Astrophys. J. Lett.* **464** (1996) L1–L4, arXiv:astro-ph/9601067.

[44] G. F. Smoot *et al.*, "Structure in the COBE Differential Microwave Radiometer First-Year Maps," *ApJS* **396** (September, 1992) L1.

[45] WMAP Collaboration, "Nine-year Wilkinson Microwave Anisotropy Probe (WMAP) Observations: Final Maps and Results," *ApJS* **208** no. 2, (October, 2013) 20, arXiv:1212.5225 [astro-ph.CO].

[46] WMAP Collaboration, "Nine-year Wilkinson Microwave Anisotropy Probe (WMAP) Observations: Cosmological Parameter Results," *ApJS* **208** no. 2, (October, 2013) 19, arXiv:1212.5226 [astro-ph.CO].

[47] Planck Collaboration, "Planck 2018 results. I. Overview and the cosmological legacy of Planck," *Astron. Astrophys.* **641** (2020) A1, arXiv:1807.06205 [astro-ph.CO].

[48] A. Liddle, *An introduction to modern cosmology; 3rd ed.* Wiley, Chichester, Mar, 2015. https://cds.cern.ch/record/1976476.

[49] Planck Collaboration, "Planck 2018 results. VI. Cosmological parameters," *Astron. Astrophys.* **641** (2020) A6, arXiv:1807.06209 [astro-ph.CO].

[50] H. Georgi and S. L. Glashow, "Unity of all elementary-particle forces," *Phys. Rev. Lett.* **32** (Feb, 1974) 438–441. https://link.aps.org/doi/10.1103/PhysRevLett.32.438.

[51] I. Aitchison, *Supersymmetry in Particle Physics. An Elementary Introduction.* Cambridge University Press, Cambridge, 2007.

[52] Muon g-2 Collaboration, "Final Report of the Muon E821 Anomalous Magnetic Moment Measurement at BNL," *Phys. Rev. D* **73** (2006) 072003, arXiv:hep-ex/0602035.

[53] H. Baer and X. Tata, *Weak Scale Supersymmetry: From Superfields to Scattering Events.* Cambridge University Press, 2006.

[54] T. Aoyama *et al.*, "The anomalous magnetic moment of the muon in the Standard Model," *Phys. Rept.* **887** (2020) 1–166, arXiv:2006.04822 [hep-ph].

[55] Muon g-2 Collaboration, "Measurement of the Positive Muon Anomalous Magnetic Moment to 0.46 ppm," *Phys. Rev. Lett.* **126** no. 14, (2021) 141801, arXiv:2104.03281 [hep-ex].

[56] A. Czarnecki and W. J. Marciano, "The Muon anomalous magnetic moment: A Harbinger for 'new physics'," *Phys. Rev. D* **64** (2001) 013014, arXiv:hep-ph/0102122.

[57] J. L. Feng and K. T. Matchev, "Supersymmetry and the anomalous magnetic moment of the muon," *Phys. Rev. Lett.* **86** (2001) 3480–3483, arXiv:hep-ph/0102146.

[58] S. Coleman and J. Mandula, "All possible symmetries of the *s* matrix," *Phys. Rev.* **159** (Jul, 1967) 1251–1256. https://link.aps.org/doi/10.1103/PhysRev.159.1251.

[59] R. Haag, J. T. Lopuszanski, and M. Sohnius, "All Possible Generators of Supersymmetries of the s Matrix," *Nucl. Phys.* **B88** (1975) 257. [,257(1974)].

[60] J. Wess and B. Zumino, "Supergauge transformations in four dimensions," *Nucl. Phys. B* **70** (1974) 39.

[61] H. Georgi and S. L. Glashow, "Gauge theories without anomalies," *Phys. Rev. D* **6** (Jul, 1972) 429–431. https://link.aps.org/doi/10.1103/PhysRevD.6.429.

[62] S. Dimopoulos and D. W. Sutter, "The Supersymmetric flavor problem," *Nucl. Phys. B* **452** (1995) 496–512, arXiv:hep-ph/9504415.

[63] MEG Collaboration, T. Mori, "Final Results of the MEG Experiment," *Nuovo Cim. C* **39** no. 4, (2017) 325, arXiv:1606.08168 [hep-ex].

[64] H. P. Nilles, "Supersymmetry, Supergravity and Particle Physics," *Phys. Rept.* **110** (1984) 1–162.

[65] A. Lahanas and D. Nanopoulos, "The road to no-scale supergravity," *Physics Reports* **145** no. 1, (1987) 1 – 139. http://www.sciencedirect.com/science/article/pii/0370157387900342.

[66] J. L. Feng, A. Rajaraman, and F. Takayama, "Superweakly interacting massive particles," *Phys. Rev. Lett.* **91** (2003) 011302, arXiv:hep-ph/0302215.

[67] S. Y. Choi, J. Kalinowski, G. A. Moortgat-Pick, and P. M. Zerwas, "Analysis of the neutralino system in supersymmetric theories," *Eur. Phys. J. C* **22** (2001) 563–579, arXiv:hep-ph/0108117. [Addendum: Eur.Phys.J.C 23, 769–772 (2002)].

[68] Super-Kamiokande Collaboration, "Search for proton decay via $p \to e^+\pi^0$ and $p \to \mu^+\pi^0$ in 0.31 megaton-years exposure of the Super-Kamiokande water Cherenkov detector," *Phys. Rev.* **D95** no. 1, (2017) 012004, arXiv:1610.03597 [hep-ex].

[69] J. R. Ellis, "Beyond the standard model for hill walkers," in *1998 European School of High-Energy Physics*, pp. 133–196. 8, 1998. arXiv:hep-ph/9812235.

[70] J. R. Ellis, J. Hagelin, D. V. Nanopoulos, *et al.*, "Supersymmetric Relics from the Big Bang," *Nucl. Phys. B* **238** (1984) 453–476.

[71] D. O. Caldwell, R. M. Eisberg, D. M. Grumm, *et al.*, "Laboratory limits on galactic cold dark matter," *Phys. Rev. Lett.* **61** (Aug, 1988) 510–513. https://link.aps.org/doi/10.1103/PhysRevLett.61.510.

[72] M. Mori, M. M. Nojiri, K. S. Hirata, *et al.*, "Search for neutralino dark matter heavier than the *w* boson at kamiokande," *Phys. Rev. D* **48** (Dec, 1993) 5505–5518. https://link.aps.org/doi/10.1103/PhysRevD.48.5505.

[73] CDMS Collaboration, D. S. Akerib *et al.*, "Exclusion limits on the WIMP-nucleon cross section from the first run of the Cryogenic Dark Matter Search in the Soudan Underground Laboratory," *Phys. Rev. D* **72** (2005) 052009, arXiv:astro-ph/0507190.

[74] A. Djouadi, J.-L. Kneur, and G. Moultaka, "SuSpect: A Fortran code for the supersymmetric and Higgs particle spectrum in the MSSM," *Comput. Phys. Commun.* **176** (2007) 426–455, arXiv:hep-ph/0211331.

[75] C. F. Berger, J. S. Gainer, J. L. Hewett, and T. G. Rizzo, "Supersymmetry without prejudice," *Journal of High Energy Physics* **2009** no. 02, (Feb, 2009) 023–023. http://dx.doi.org/10.1088/1126-6708/2009/02/023.

[76] J. Alwall, P. Schuster, and N. Toro, "Simplified Models for a First Characterization of New Physics at the LHC," *Phys. Rev.* **D79** (2009) 075020, arXiv:0810.3921 [hep-ph].

[77] L. N. P. W. Group, "Simplified Models for LHC New Physics Searches," *J. Phys.* **G39** (2012) 105005, arXiv:1105.2838 [hep-ph].

[78] D. S. Alves, E. Izaguirre, and J. G. Wacker, "Where the Sidewalk Ends: Jets and Missing Energy Search Strategies for the 7 TeV LHC," *JHEP* **10** (2011) 012, arXiv:1102.5338 [hep-ph].

[79] F. Ambrogi, S. Kraml, S. Kulkarni, *et al.*, "On the coverage of the pMSSM by simplified model results," *Eur. Phys. J. C* **78** no. 3, (2018) 215, arXiv:1707.09036 [hep-ph].

[80] O. Buchmueller and J. Marrouche, "Universal mass limits on gluino and third-generation squarks in the context of Natural-like SUSY spectra," *Int. J. Mod. Phys. A* **29** no. 06, (2014) 1450032, arXiv:1304.2185 [hep-ph].

[81] W. Beenakker, C. Borschensky, M. Krämer, *et al.*, "NNLL-fast: predictions for coloured supersymmetric particle production at the LHC with threshold and Coulomb resummation," *JHEP* **12** (2016) 133, arXiv:1607.07741 [hep-ph].

[82] M. Beneke, M. Czakon, P. Falgari, *et al.*, "Threshold expansion of the $gg(q\bar{q}) \to Q\bar{Q} + X$ cross section at $\mathcal{O}(\alpha_s^4)$," *Phys. Lett. B* **690** (2010) 483, arXiv:0911.5166 [hep-ph].

[83] J. Fiaschi and M. Klasen, "Neutralino-chargino pair production at NLO+NLL with resummation-improved parton density functions for LHC Run II," *Phys. Rev. D* **98** no. 5, (2018) 055014, arXiv:1805.11322 [hep-ph].

[84] B. Fuks, M. Klasen, D. R. Lamprea, and M. Rothering, "Gaugino production in proton-proton collisions at a center-of-mass energy of 8 TeV," *JHEP* **10** (2012) 081, arXiv:1207.2159 [hep-ph].

[85] J. Fiaschi and M. Klasen, "Slepton pair production at the LHC in NLO+NLL with resummation-improved parton densities," *JHEP* **03** (2018) 094, arXiv:1801.10357 [hep-ph].

[86] ATLAS Collaboration, M. Aaboud *et al.*, "Dark matter interpretations of ATLAS searches for the electroweak production of supersymmetric particles in $\sqrt{s} = 8$ TeV proton-proton collisions," *JHEP* **09** (2016) 175, arXiv:1608.00872 [hep-ex].

[87] ATLAS Collaboration, "Summary of the ATLAS experiment's sensitivity to supersymmetry after LHC Run 1 — interpreted in the phenomenological MSSM," *JHEP* **10** (2015) 134, arXiv:1508.06608 [hep-ex].

[88] ATLAS Collaboration, "Mass reach of the atlas searches for supersymmetry." https://atlas.web.cern.ch/Atlas/GROUPS/PHYSICS/PUBNOTES/ATL-PHYS-PUB-2020-020/fig_23.png, 2020.

[89] CMS Collaboration, "Summary plot moriond 2017." https://twiki.cern.ch/twiki/pub/CMSPublic/SUSYSummary2017/Moriond2017_BarPlot.pdf, 2017.

[90] L. S. W. Group, "Notes lepsusywg/02-04.1 and lepsusywg/01-03.1." http://lepsusy.web.cern.ch/lepsusy/, 2004. Accessed: 2021-02-11.

[91] ATLAS Collaboration, "Searches for electroweak production of supersymmetric particles with compressed mass spectra in $\sqrt{s} = 13$ TeV pp collisions with the ATLAS detector," *Phys. Rev. D* **101** (2020) 052005, arXiv:1911.12606 [hep-ex].

[92] ATLAS Collaboration, "Observation of a new particle in the search for the Standard Model Higgs boson with the ATLAS detector at the LHC," *Phys. Lett. B* **716** (2012) 1–29, arXiv:1207.7214 [hep-ex].

[93] CMS Collaboration, "Observation of a New Boson at a Mass of 125 GeV with the CMS Experiment at the LHC," *Phys. Lett. B* **716** (2012) 30–61, arXiv:1207.7235 [hep-ex].

[94] A. Buckley, "PySLHA: a Pythonic interface to SUSY Les Houches Accord data," *Eur. Phys. J. C* **75** no. 10, (2015) 467, arXiv:1305.4194 [hep-ph].

[95] CERN, "About cern." https://home.cern/about. Accessed: 2021-01-21.

[96] CERN, "CERN Annual report 2019," tech. rep., CERN, Geneva, 2020. https://cds.cern.ch/record/2723123.

[97] O. S. Bruning, P. Collier, P. Lebrun, *et al.*, *LHC Design Report*. CERN Yellow Reports: Monographs. CERN, Geneva, 2004. https://cds.cern.ch/record/782076.

[98] M. Blewett and N. Vogt-Nilsen, "Proceedings of the 8th international conference on high-energy accelerators, cern 1971. conference held at geneva, 20–24 september 1971.," tech. rep., 1971, 1971.

[99] L. R. Evans and P. Bryant, "LHC Machine," *JINST* **3** (2008) S08001. 164 p. http://cds.cern.ch/record/1129806. This report is an abridged version of the LHC Design Report (CERN-2004-003).

[100] R. Scrivens, M. Kronberger, D. Küchler, *et al.*, "Overview of the status and developments on primary ion sources at CERN*,". https://cds.cern.ch/record/1382102.

[101] M. Vretenar, J. Vollaire, R. Scrivens, *et al.*, *Linac4 design report*, vol. 6 of *CERN Yellow Reports: Monographs*. CERN, Geneva, 2020. https://cds.cern.ch/record/2736208.

[102] E. Mobs, "The CERN accelerator complex - 2019. Complexe des accélérateurs du CERN - 2019,". https://cds.cern.ch/record/2684277. General Photo.

[103] ATLAS Collaboration, "The ATLAS Experiment at the CERN Large Hadron Collider," *JINST* **3** (2008) S08003.

[104] CMS Collaboration, "The CMS Experiment at the CERN LHC," *JINST* **3** (2008) S08004.

[105] ALICE Collaboration, "The ALICE experiment at the CERN LHC," *JINST* **3** (2008) S08002.

[106] LHCb Collaboration, "The LHCb Detector at the LHC," *JINST* **3** (2008) S08005.

[107] TOTEM Collaboration, "The TOTEM experiment at the CERN Large Hadron Collider," *JINST* **3** (2008) S08007.

[108] LHCf Collaboration, "Technical design report of the LHCf experiment: Measurement of photons and neutral pions in the very forward region of LHC,".

[109] MoEDAL Collaboration, "Technical Design Report of the MoEDAL Experiment,".

[110] ATLAS Collaboration, "ATLAS Public Results - Luminosity Public Results Run 2,". https://twiki.cern.ch/twiki/bin/view/AtlasPublic/LuminosityPublicResultsRun2. Accessed: 2021-01-17.

[111] ATLAS Collaboration, Z. Marshall, "Simulation of Pile-up in the ATLAS Experiment," *J. Phys. Conf. Ser.* **513** (2014) 022024.

[112] "First beam in the LHC - accelerating science,". https://home.cern/news/news/accelerators/record-luminosity-well-done-lhc. Accessed: 2021-01-10.

[113] ATLAS Collaboration, "Luminosity determination in pp collisions at $\sqrt{s}$ = 13 TeV using the ATLAS detector at the LHC," Tech. Rep. ATLAS-CONF-2019-021, CERN, Geneva, Jun, 2019. https://cds.cern.ch/record/2677054.

[114] ATLAS Collaboration, "Luminosity determination in pp collisions at $\sqrt{s}$ = 8 TeV using the ATLAS detector at the LHC," *Eur. Phys. J. C* **76** no. 12, (2016) 653, arXiv:1608.03953 [hep-ex].

[115] G. Avoni, M. Bruschi, G. Cabras, *et al.*, "The new LUCID-2 detector for luminosity measurement and monitoring in ATLAS," *Journal of Instrumentation* **13** no. 07, (Jul, 2018) P07017–P07017. https://doi.org/10.1088/1748-0221/13/07/p07017.

[116] S. van der Meer, "Calibration of the effective beam height in the ISR," Tech. Rep. CERN-ISR-PO-68-31. ISR-PO-68-31, CERN, Geneva, 1968. https://cds.cern.ch/record/296752.

[117] P. Grafström and W. Kozanecki, "Luminosity determination at proton colliders," *Progress in Particle and Nuclear Physics* **81** (2015) 97 – 148. http://www.sciencedirect.com/science/article/pii/S0146641014000878.

[118] M. Bajko *et al.*, "Report of the Task Force on the Incident of 19th September 2008 at the LHC," Tech. Rep. LHC-PROJECT-Report-1168. CERN-LHC-PROJECT-Report-1168, CERN, Geneva, Mar, 2009. https://cds.cern.ch/record/1168025.

[119] "New schedule for CERN's accelerators and experiments,". https://home.cern/news/press-release/cern/first-beam-lhc-accelerating-science. Accessed: 2021-01-10.

[120] ATLAS Collaboration, "Luminosity Determination in pp Collisions at $\sqrt{s}$ = 7 TeV Using the ATLAS Detector at the LHC," *Eur. Phys. J. C* **71** (2011) 1630, arXiv:1101.2185 [hep-ex].

[121] ATLAS Collaboration, "Improved luminosity determination in pp collisions at $\sqrt{s}$ = 7 TeV using the ATLAS detector at the LHC.," *Eur. Phys. J. C* **73** no. CERN-PH-EP-2013-026, (Feb, 2013) 2518. 27 p. https://cds.cern.ch/record/1517411.

[122] "Record luminosity: well done LHC,". https://home.cern/news/news/accelerators/new-schedule-cerns-accelerators-and-experiments. Accessed: 2021-01-10.

[123] CERN, "New schedule for CERN's accelerators and experiments," November, 2020. https://home.cern/news/news/accelerators/new-schedule-cerns-accelerators-and-experiments. Accessed: 2021-03-12.

[124] A. G., B. A. I., B. O., *et al.*, *High-Luminosity Large Hadron Collider (HL-LHC): Technical Design Report V. 0.1*. CERN Yellow Reports: Monographs. CERN, Geneva, 2017. https://cds.cern.ch/record/2284929.

[125] J. Pequenao, "Computer generated image of the whole ATLAS detector." Mar, 2008.

[126] ATLAS Collaboration, "ATLAS: Detector and physics performance technical design report. Volume 1,".

[127] J. Pequenao, "Computer generated image of the ATLAS inner detector." Mar, 2008.

[128] ATLAS Collaboration, K. Potamianos, "The upgraded Pixel detector and the commissioning of the Inner Detector tracking of the ATLAS experiment for Run-2 at the Large Hadron Collider," Tech. Rep. ATL-PHYS-PROC-2016-104, CERN, Geneva, Aug, 2016. https://cds.cern.ch/record/2209070. 15 pages, EPS-HEP 2015 Proceedings.

[129] ATLAS IBL Collaboration, "Production and Integration of the ATLAS Insertable B-Layer," *JINST* **13** no. 05, (2018) T05008, arXiv:1803.00844 [physics.ins-det].

[130] ATLAS Collaboration, "ATLAS Insertable B-Layer Technical Design Report," Tech. Rep. CERN-LHCC-2010-013. ATLAS-TDR-19, Sep, 2010. http://cds.cern.ch/record/1291633.

[131] ATLAS Collaboration, "ATLAS b-jet identification performance and efficiency measurement with $t\bar{t}$ events in pp collisions at $\sqrt{s}$ = 13 TeV," *Eur. Phys. J. C* **79** no. 11, (2019) 970, arXiv:1907.05120 [hep-ex].

[132] ATLAS Collaboration, "Particle Identification Performance of the ATLAS Transition Radiation Tracker." ATLAS-CONF-2011-128, 2011. https://cds.cern.ch/record/1383793.

[133] J. Pequenao, "Computer Generated image of the ATLAS calorimeter." Mar, 2008.

[134] J. Pequenao, "Computer generated image of the ATLAS Muons subsystem." Mar, 2008.

[135] S. Lee, M. Livan, and R. Wigmans, "Dual-Readout Calorimetry," *Rev. Mod. Phys.* **90** no. arXiv:1712.05494. 2, (Dec, 2017) 025002. 40 p. https://cds.cern.ch/record/2637852. 44 pages, 53 figures, accepted for publication in Review of Modern Physics.

[136] M. Leite, "Performance of the ATLAS Zero Degree Calorimeter," Tech. Rep. ATL-FWD-PROC-2013-001, CERN, Geneva, Nov, 2013. https://cds.cern.ch/record/1628749.

[137] S. Abdel Khalek *et al.*, "The ALFA Roman Pot Detectors of ATLAS," *JINST* **11** no. 11, (2016) P11013, arXiv:1609.00249 [physics.ins-det].

[138] U. Amaldi, G. Cocconi, A. Diddens, *et al.*, "The real part of the forward proton proton scattering amplitude measured at the cern intersecting storage rings," *Physics Letters B* **66** no. 4, (1977) 390 – 394. http://www.sciencedirect.com/science/article/pii/0370269377900223.

[139] L. Adamczyk, E. Banaś, A. Brandt, *et al.*, "Technical Design Report for the ATLAS Forward Proton Detector," Tech. Rep. CERN-LHCC-2015-009. ATLAS-TDR-024, May, 2015. https://cds.cern.ch/record/2017378.

[140] ATLAS Collaboration, A. R. Martínez, "The Run-2 ATLAS Trigger System," *J. Phys. Conf. Ser.* **762** no. 1, (2016) 012003.

[141] ATLAS Collaboration, *ATLAS level-1 trigger: Technical Design Report.* Technical Design Report ATLAS. CERN, Geneva, 1998. https://cds.cern.ch/record/381429.

[142] ATLAS Collaboration, "Operation of the ATLAS trigger system in Run 2," *JINST* **15** no. 10, (2020) P10004, arXiv:2007.12539 [physics.ins-det].

[143] ATLAS Collaboration, P. Jenni, M. Nessi, M. Nordberg, and K. Smith, *ATLAS high-level trigger, data-acquisition and controls: Technical Design Report.* Technical Design Report ATLAS. CERN, Geneva, 2003. https://cds.cern.ch/record/616089.

[144] ATLAS Collaboration, "The ATLAS Simulation Infrastructure," *Eur. Phys. J. C* **70** (2010) 823–874, arXiv:1005.4568 [physics.ins-det].

[145] T. Gleisberg, S. Hoeche, F. Krauss, *et al.*, "Event generation with SHERPA 1.1," *JHEP* **02** (2009) 007, arXiv:0811.4622 [hep-ph].

[146] A. Buckley *et al.*, "General-purpose event generators for LHC physics," *Phys. Rept.* **504** (2011) 145–233, arXiv:1101.2599 [hep-ph].

[147] V. N. Gribov and L. N. Lipatov, "Deep inelastic e p scattering in perturbation theory," *Sov. J. Nucl. Phys.* **15** (1972) 438–450.

[148] J. Blumlein, T. Doyle, F. Hautmann, *et al.*, "Structure functions in deep inelastic scattering at HERA," in *Workshop on Future Physics at HERA (To be followed by meetings 7-9 Feb and 30-31 May 1996 at DESY)*. 9, 1996. arXiv:hep-ph/9609425.

[149] A. Buckley, J. Ferrando, S. Lloyd, *et al.*, "LHAPDF6: parton density access in the LHC precision era," *Eur. Phys. J. C* **75** (2015) 132, arXiv:1412.7420 [hep-ph].

[150] M. Bengtsson and T. Sjostrand, "Coherent Parton Showers Versus Matrix Elements: Implications of PETRA - PEP Data," *Phys. Lett. B* **185** (1987) 435.

[151] S. Catani, F. Krauss, R. Kuhn, and B. R. Webber, "QCD matrix elements + parton showers," *JHEP* **11** (2001) 063, arXiv:hep-ph/0109231.

[152] L. Lonnblad, "Correcting the color dipole cascade model with fixed order matrix elements," *JHEP* **05** (2002) 046, arXiv:hep-ph/0112284.

[153] B. Andersson, G. Gustafson, G. Ingelman, and T. Sjostrand, "Parton Fragmentation and String Dynamics," *Phys. Rept.* **97** (1983) 31–145.

[154] B. Andersson, *The Lund Model*. Cambridge Monographs on Particle Physics, Nuclear Physics and Cosmology. Cambridge University Press, 1998.

[155] D. Amati and G. Veneziano, "Preconfinement as a Property of Perturbative QCD," *Phys. Lett. B* **83** (1979) 87–92.

[156] D. Yennie, S. Frautschi, and H. Suura, "The infrared divergence phenomena and high-energy processes," *Annals of Physics* **13** no. 3, (1961) 379–452. https://www.sciencedirect.com/science/article/pii/0003491661901518.

[157] M. Dobbs and J. B. Hansen, "The HepMC C++ Monte Carlo event record for High Energy Physics," *Comput. Phys. Commun.* **134** (2001) 41–46.

[158] GEANT4 Collaboration, "GEANT4: A Simulation toolkit," *Nucl. Instrum. Meth.* **A506** (2003) 250–303.

[159] ATLAS Collaboration, "The new Fast Calorimeter Simulation in ATLAS," Tech. Rep. ATL-SOFT-PUB-2018-002, CERN, Geneva, Jul, 2018. https://cds.cern.ch/record/2630434.

[160] K. Cranmer, "Practical Statistics for the LHC," in *2011 European School of High-Energy Physics*, pp. 267–308. 2014. arXiv:1503.07622 [physics.data-an].

[161] G. Cowan, K. Cranmer, E. Gross, and O. Vitells, "Asymptotic formulae for likelihood-based tests of new physics," *Eur. Phys. J.* **C71** (2011) 1554, arXiv:1007.1727 [physics.data-an]. [Erratum: Eur. Phys. J.C73,2501(2013)].

[162] ATLAS Collaboration, "Reproduction searches for new physics with the ATLAS experiment through publication of full statistical likelihoods." ATL-PHYS-PUB-2019-029, 2019. https://cds.cern.ch/record/2684863.

[163] ROOT Collaboration, K. Cranmer, G. Lewis, L. Moneta, *et al.*, "HistFactory: A tool for creating statistical models for use with RooFit and RooStats," Tech. Rep. CERN-OPEN-2012-016, New York U., New York, Jan, 2012. https://cds.cern.ch/record/1456844.

[164] W. Verkerke and D. P. Kirkby, "The RooFit toolkit for data modeling," *eConf* **C0303241** (2003) MOLT007, arXiv:physics/0306116 [physics]. [,186(2003)].

[165] F. James and M. Roos, "MINUIT: a system for function minimization and analysis of the parameter errors and corrections," *Comput. Phys. Commun.* **10** no. CERN-DD-75-20, (Jul, 1975) 343–367. 38 p. https://cds.cern.ch/record/310399.

[166] L. Moneta, K. Belasco, K. S. Cranmer, *et al.*, "The RooStats Project," *PoS* **ACAT2010** (2010) 057, arXiv:1009.1003 [physics.data-an].

[167] R. Brun and F. Rademakers, "ROOT: An object oriented data analysis framework," *Nucl. Instrum. Meth.* **A389** (1997) 81–86.

[168] I. Antcheva *et al.*, "ROOT — A C++ framework for petabyte data storage, statistical analysis and visualization," *Computer Physics Communications* **182** no. 6, (2011) 1384 – 1385. http://www.sciencedirect.com/science/article/pii/S0010465511000701.

[169] M. Baak, G. J. Besjes, D. Côte, A. Koutsman, J. Lorenz, D. Short, "HistFitter software framework for statistical data analysis," *Eur. Phys. J.* **C75** (2015) 153, arXiv:1410.1280 [hep-ex].

[170] L. Heinrich, M. Feickert, G. Stark, and K. Cranmer, "pyhf: pure-python implementation of histfactory statistical models," *Journal of Open Source Software* **6** no. 58, (2021) 2823. https://doi.org/10.21105/joss.02823.

[171] L. Heinrich, M. Feickert, and G. Stark, "pyhf: v0.6.0," Version 0.6.0. https://github.com/scikit-hep/pyhf.

[172] C. R. Harris, K. J. Millman, S. J. van der Walt, *et al.*, "Array programming with NumPy," *Nature* **585** no. 7825, (Sept., 2020) 357–362. https://doi.org/10.1038/s41586-020-2649-2.

[173] A. Paszke, S. Gross, F. Massa, *et al.*, "Pytorch: An imperative style, high-performance deep learning library," in *Advances in Neural Information Processing Systems 32*, H. Wallach, H. Larochelle, A. Beygelzimer, *et al.*, eds., pp. 8024–8035. Curran Associates, Inc., 2019. http://papers.neurips.cc/paper/9015-pytorch-an-imperative-style-high-performance-deep-learning-library.pdf.

[174] M. Abadi, A. Agarwal, P. Barham, *et al.*, "TensorFlow: Large-scale machine learning on heterogeneous systems," 2015. https://www.tensorflow.org/. Software available from tensorflow.org.

[175] J. Bradbury, R. Frostig, P. Hawkins, *et al.*, "JAX: composable transformations of Python+NumPy programs," Version 0.1.46, 2018. http://github.com/google/jax.

[176] S. S. Wilks, "The large-sample distribution of the likelihood ratio for testing composite hypotheses," *Ann. Math. Statist.* **9** no. 1, (03, 1938) 60–62. https://doi.org/10.1214/aoms/1177732360.

[177] A. Wald, "Tests of statistical hypotheses concerning several parameters when the number of observations is large," *Transactions of the American Mathematical Society* **54** no. 3, (1943) 426–482. https://doi.org/10.1090/S0002-9947-1943-0012401-3.

[178] G. Cowan, "Statistics for Searches at the LHC," in *69th Scottish Universities Summer School in Physics: LHC Physics*, pp. 321–355. 7, 2013. arXiv:1307.2487 [hep-ex].

[179] A. L. Read, "Presentation of search results: the CL_S technique," *J. Phys. G* **28** (2002) 2693.

[180] R. D. Cousins, J. T. Linnemann, and J. Tucker, "Evaluation of three methods for calculating statistical significance when incorporating a systematic uncertainty into a test of the background-only hypothesis for a Poisson process," *Nucl. Instrum. Meth. A* **595** no. 2, (2008) 480, arXiv:physics/0702156 [physics.data-an].

[181] K. Cranmer, "Statistical challenges for searches for new physics at the LHC," in *Statistical Problems in Particle Physics, Astrophysics and Cosmology (PHYSTAT 05): Proceedings, Oxford, UK, September 12-15, 2005*, pp. 112–123. 2005. arXiv:physics/0511028 [physics.data-an]. http://www.physics.ox.ac.uk/phystat05/proceedings/files//Cranmer_LHCStatisticalChallenges.ps.

[182] ATLAS Collaboration, "Search for direct pair production of a chargino and a neutralino decaying to the 125 GeV Higgs boson in $\sqrt{s} = 8$ TeV pp collisions with the ATLAS detector," *Eur. Phys. J. C* **75** (2015) 208, arXiv:1501.07110 [hep-ex].

[183] ATLAS Collaboration, "Search for chargino and neutralino production in final states with a Higgs boson and missing transverse momentum at $\sqrt{s} = 13$ TeV with the ATLAS detector," *Phys. Rev. D* **100** (2019) 012006, arXiv:1812.09432 [hep-ex].

[184] CMS Collaboration, "Search for electroweak production of charginos and neutralinos in WH events in proton–proton collisions at $\sqrt{s} = 13$ TeV," *JHEP* **11** (2017) 029, arXiv:1706.09933 [hep-ex].

[185] ATLAS Collaboration, "Search for direct production of electroweakinos in final states with one lepton, missing transverse momentum and a Higgs boson decaying into two b-jets in pp collisions at $\sqrt{s} = 13$ TeV with the ATLAS detector," *Eur. Phys. J. C* **80** (2020) 691, arXiv:1909.09226 [hep-ex].

[186] ATLAS Collaboration, "Improvements in $t\bar{t}$ modelling using NLO+PS Monte Carlo generators for Run 2." ATL-PHYS-PUB-2018-009, 2018. https://cds.cern.ch/record/2630327.

[187] ATLAS Collaboration, "Modelling of the $t\bar{t}H$ and $t\bar{t}V(V = W, Z)$ processes for $\sqrt{s} = 13$ TeV ATLAS analyses." ATL-PHYS-PUB-2016-005, 2016. https://cds.cern.ch/record/2120826.

[188] ATLAS Collaboration, "ATLAS simulation of boson plus jets processes in Run 2." ATL-PHYS-PUB-2017-006, 2017. https://cds.cern.ch/record/2261937.

[189] ATLAS Collaboration, "Multi-Boson Simulation for 13 TeV ATLAS Analyses." ATL-PHYS-PUB-2017-005, 2017. https://cds.cern.ch/record/2261933.

[190] J. Alwall, R. Frederix, S. Frixione, *et al.*, "The automated computation of tree-level and next-to-leading order differential cross sections, and their matching to parton shower simulations," *JHEP* **07** (2014) 079, arXiv:1405.0301 [hep-ph].

[191] R. Frederix and S. Frixione, "Merging meets matching in MC@NLO," *JHEP* **12** (2012) 061, arXiv:1209.6215 [hep-ph].

[192] "Parton distributions with LHC data," *Nucl. Phys. B* **867** (2013) 244, arXiv:1207.1303 [hep-ph].

[193] T. Sjöstrand, S. Ask, J. R. Christiansen, *et al.*, "An Introduction to PYTHIA 8.2," *Comput. Phys. Commun.* **191** (2015) 159–177, arXiv:1410.3012 [hep-ph].

[194] ATLAS Collaboration, "ATLAS Pythia 8 tunes to 7 TeV data." ATL-PHYS-PUB-2014-021, 2014. https://cds.cern.ch/record/1966419.

[195] L. Lönnblad and S. Prestel, "Matching tree-level matrix elements with interleaved showers," *JHEP* **03** (2012) 019, arXiv:1109.4829 [hep-ph].

[196] D. J. Lange, "The EvtGen particle decay simulation package," *Nucl. Instrum. Meth. A* **462** (2001) 152.

[197] ATLAS Collaboration, "The Pythia 8 A3 tune description of ATLAS minimum bias and inelastic measurements incorporating the Donnachie–Landshoff diffractive model." ATL-PHYS-PUB-2016-017, 2016. https://cds.cern.ch/record/2206965.

[198] B. Fuks, M. Klasen, D. R. Lamprea, and M. Rothering, "Precision predictions for electroweak superpartner production at hadron colliders with RESUMMINO," *Eur. Phys. J. C* **73** (2013) 2480, arXiv:1304.0790 [hep-ph].

[199] S. Alioli, P. Nason, C. Oleari, and E. Re, "A general framework for implementing NLO calculations in shower Monte Carlo programs: the POWHEG BOX," *JHEP* **06** (2010) 043, arXiv:1002.2581 [hep-ph].

[200] S. Frixione, P. Nason, and G. Ridolfi, "A Positive-weight next-to-leading-order Monte Carlo for heavy flavour hadroproduction," *JHEP* **09** (2007) 126, arXiv:0707.3088 [hep-ph].

[201] P. Nason, "A New method for combining NLO QCD with shower Monte Carlo algorithms," *JHEP* **11** (2004) 040, arXiv:hep-ph/0409146.

[202] E. Bothmann *et al.*, "Event generation with Sherpa 2.2," *SciPost Phys.* **7** no. 3, (2019) 034, arXiv:1905.09127 [hep-ph].

[203] NNPDF Collaboration, "Parton distributions for the LHC run II," *JHEP* **04** (2015) 040, arXiv:1410.8849 [hep-ph].

[204] M. Czakon and A. Mitov, "Top++: A program for the calculation of the top-pair cross-section at hadron colliders," *Comput. Phys. Commun.* **185** (2014) 2930, arXiv:1112.5675 [hep-ph].

[205] M. Cacciari, M. Czakon, M. Mangano, *et al.*, "Top-pair production at hadron colliders with next-to-next-to-leading logarithmic soft-gluon resummation," *Phys. Lett. B* **710** (2012) 612–622, arXiv:1111.5869 [hep-ph].

[206] P. Kant, O. M. Kind, T. Kintscher, *et al.*, "HatHor for single top-quark production: Updated predictions and uncertainty estimates for single top-quark production in hadronic collisions," *Comput. Phys. Commun.* **191** (2015) 74–89, arXiv:1406.4403 [hep-ph].

[207] N. Kidonakis, "Two-loop soft anomalous dimensions for single top quark associated production with a W^- or H^-," *Phys. Rev. D* **82** (2010) 054018, arXiv:1005.4451 [hep-ph].

[208] J. M. Campbell and R. K. Ellis, "$t\bar{t}W^{+-}$ production and decay at NLO," *JHEP* **07** (2012) 052, arXiv:1204.5678 [hep-ph].

[209] A. Lazopoulos, T. McElmurry, K. Melnikov, and F. Petriello, "Next-to-leading order QCD corrections to $t\bar{t}Z$ production at the LHC," *Phys. Lett. B* **666** (2008) 62–65, arXiv:0804.2220 [hep-ph].

[210] R. Gavin, Y. Li, F. Petriello, and S. Quackenbush, "FEWZ 2.0: A code for hadronic Z production at next-to-next-to-leading order," arXiv:1011.3540 [hep-ph].

[211] LHC Higgs Cross Section Working Group Collaboration, "Handbook of LHC Higgs Cross Sections: 4. Deciphering the Nature of the Higgs Sector," arXiv:1610.07922 [hep-ph].

[212] ATLAS Collaboration, "Example ATLAS tunes of PYTHIA8, PYTHIA6 and POWHEG to an observable sensitive to Z boson transverse momentum." ATL-PHYS-PUB-2013-017, 2013. https://cds.cern.ch/record/1629317.

[213] ATLAS Collaboration, "Performance of the ATLAS track reconstruction algorithms in dense environments in LHC Run 2," *Eur. Phys. J. C* **77** (2017) 673, arXiv:1704.07983 [hep-ex].

[214] R. Frühwirth, "Application of Kalman filtering to track and vertex fitting," *Nucl. Instrum. Methods Phys. Res., A* **262** no. HEPHY-PUB-503, (Jun, 1987) 444. 19 p. https://cds.cern.ch/record/178627.

[215] T. Cornelissen, M. Elsing, I. Gavrilenko, *et al.*, "The new ATLAS track reconstruction (NEWT)," *J. Phys.: Conf. Ser.* **119** (2008) 032014. https://cds.cern.ch/record/1176900.

[216] ATLAS Collaboration, "Vertex Reconstruction Performance of the ATLAS Detector at $\sqrt{s}$ = 13 TeV." ATL-PHYS-PUB-2015-026, 2015. https://cds.cern.ch/record/2037717.

[217] ATLAS Collaboration, "Reconstruction of primary vertices at the ATLAS experiment in Run 1 proton–proton collisions at the LHC," *Eur. Phys. J. C* **77** (2017) 332, arXiv:1611.10235 [hep-ex].

[218] ATLAS Collaboration, "Topological cell clustering in the ATLAS calorimeters and its performance in LHC Run 1," *Eur. Phys. J. C* **77** (2017) 490, arXiv:1603.02934 [hep-ex].

[219] ATLAS Collaboration, "Electron and photon performance measurements with the ATLAS detector using the 2015–2017 LHC proton–proton collision data," *JINST* **14** (2019) P12006, arXiv:1908.00005 [hep-ex].

[220] ATLAS Collaboration, "Measurement of the photon identification efficiencies with the ATLAS detector using LHC Run 2 data collected in 2015 and 2016," *Eur. Phys. J. C* **79** (2019) 205, arXiv:1810.05087 [hep-ex].

[221] ATLAS Collaboration, "Electron reconstruction and identification in the ATLAS experiment using the 2015 and 2016 LHC proton–proton collision data at $\sqrt{s}$ = 13 TeV," *Eur. Phys. J. C* **79** (2019) 639, arXiv:1902.04655 [hep-ex].

[222] ATLAS Collaboration, "Muon reconstruction performance of the ATLAS detector in proton–proton collision data at $\sqrt{s}$ = 13 TeV," *Eur. Phys. J. C* **76** (2016) 292, arXiv:1603.05598 [hep-ex].

[223] ATLAS Collaboration, "Muon reconstruction and identification efficiency in ATLAS using the full Run 2 *pp* collision data set at $\sqrt{s}$ = 13 TeV," arXiv:2012.00578 [hep-ex].

[224] M. Cacciari, G. P. Salam, and G. Soyez, "The anti-k_t jet clustering algorithm," *JHEP* **04** (2008) 063, arXiv:0802.1189 [hep-ph].

[225] M. Cacciari, G. P. Salam, and G. Soyez, "FastJet user manual," *Eur. Phys. J. C* **72** (2012) 1896, arXiv:1111.6097 [hep-ph].

[226] M. Cacciari, "FastJet: A Code for fast k_t clustering, and more," in *Deep inelastic scattering. Proceedings, 14th International Workshop, DIS 2006, Tsukuba, Japan, April 20-24, 2006*, pp. 487–490. 2006. arXiv:hep-ph/0607071 [hep-ph]. [,125(2006)].

[227] ATLAS Collaboration, "Jet energy scale and resolution measured in proton-proton collisions at $\sqrt{s}$ = 13 TeV with the ATLAS detector," arXiv:2007.02645 [hep-ex].

[228] M. Cacciari and G. P. Salam, "Pileup subtraction using jet areas," *Phys. Lett. B* **659** (2008) 119–126, arXiv:0707.1378 [hep-ph].

[229] ATLAS Collaboration, "Jet energy measurement with the ATLAS detector in proton–proton collisions at $\sqrt{s}$ = 7 TeV," *Eur. Phys. J. C* **73** (2013) 2304, arXiv:1112.6426 [hep-ex].

[230] ATLAS Collaboration, "Determination of jet calibration and energy resolution in proton–proton collisions at $\sqrt{s}$ = 8 TeV using the ATLAS detector," arXiv:1910.04482 [hep-ex].

[231] ATLAS Collaboration, "Performance of pile-up mitigation techniques for jets in *pp* collisions at $\sqrt{s}$ = 8 TeV using the ATLAS detector," *Eur. Phys. J. C* **76** (2016) 581, arXiv:1510.03823 [hep-ex].

[232] ATLAS Collaboration, "Optimisation and performance studies of the ATLAS *b*-tagging algorithms for the 2017-18 LHC run." ATL-PHYS-PUB-2017-013, 2017. https://cds.cern.ch/record/2273281.

[233] ATLAS Collaboration, "ATLAS b-jet identification performance and efficiency measurement with $t\bar{t}$ events in pp collisions at $\sqrt{s} = 13$ TeV," *Eur. Phys. J. C* **79** (2019) 970, arXiv:1907.05120 [hep-ex].

[234] ATLAS Collaboration, "Measurements of b-jet tagging efficiency with the ATLAS detector using $t\bar{t}$ events at $\sqrt{s} = 13$ TeV," *JHEP* **08** (2018) 089, arXiv:1805.01845 [hep-ex].

[235] ATLAS Collaboration, "Performance of missing transverse momentum reconstruction with the ATLAS detector using proton–proton collisions at $\sqrt{s} = 13$ TeV," *Eur. Phys. J. C* **78** (2018) 903, arXiv:1802.08168 [hep-ex].

[236] ATLAS Collaboration, "$E_{\mathrm{T}}^{\mathrm{miss}}$ performance in the ATLAS detector using 2015-2016 LHC p-p collisions," Tech. Rep. ATLAS-CONF-2018-023, CERN, Geneva, Jun, 2018. http://cds.cern.ch/record/2625233.

[237] D. Adams *et al.*, "Recommendations of the Physics Objects and Analysis Harmonisation Study Groups 2014," Tech. Rep. ATL-PHYS-INT-2014-018, CERN, Geneva, Jul, 2014. https://cds.cern.ch/record/1743654.

[238] M. Cacciari, G. P. Salam, and G. Soyez, "The Catchment Area of Jets," *JHEP* **04** (2008) 005, arXiv:0802.1188 [hep-ph].

[239] UA1 Collaboration, "Experimental Observation of Isolated Large Transverse Energy Electrons with Associated Missing Energy at $\sqrt{s} = 540$ GeV," *Phys. Lett. B* **122** (1983) 103–116.

[240] Aachen-Annecy-Birmingham-CERN-Helsinki-London(QMC)-Paris(CdF)-Riverside-Rome-Rutherford-Saclay(CEN)-Vienna Collaboration, G. Arnison *et al.*, "Further evidence for charged intermediate vector bosons at the SPS collider," *Phys. Lett. B* **129** no. CERN-EP-83-111, (Jun, 1985) 273–282. 17 p. https://cds.cern.ch/record/163856.

[241] U. Baur, "Measuring the W boson mass at hadron colliders," in *Mini-Workshop on Electroweak Precision Data and the Higgs Mass*. 4, 2003. arXiv:hep-ph/0304266.

[242] J. Smith, W. L. van Neerven, and J. A. M. Vermaseren, "The Transverse Mass and Width of the W Boson," *Phys. Rev. Lett.* **50** (1983) 1738.

[243] D. R. Tovey, "On measuring the masses of pair-produced semi-invisibly decaying particles at hadron colliders," *JHEP* **04** (2008) 034, arXiv:0802.2879 [hep-ph].

[244] G. Polesello and D. R. Tovey, "Supersymmetric particle mass measurement with the boost-corrected contransverse mass," *JHEP* **03** (2010) 030, arXiv:0910.0174 [hep-ph].

[245] ATLAS Collaboration, "Performance of the missing transverse momentum triggers for the ATLAS detector during Run-2 data taking," *JHEP* **08** (2020) 080, arXiv:2005.09554 [hep-ex].

[246] ATLAS Collaboration, "Performance of algorithms that reconstruct missing transverse momentum in $\sqrt{s} = 8$ TeV proton-proton collisions in the ATLAS detector," *Eur. Phys. J. C* **77** no. 4, (2017) 241, arXiv:1609.09324 [hep-ex].

[247] ATLAS Collaboration, "ATLAS data quality operations and performance for 2015–2018 data-taking," *JINST* **15** (2020) P04003, arXiv:1911.04632 [physics.ins-det].

[248] ATLAS Collaboration, "Selection of jets produced in 13 TeV proton–proton collisions with the ATLAS detector." ATLAS-CONF-2015-029, 2015. https://cds.cern.ch/record/2037702.

[249] N. Hartmann, "ahoi." https://gitlab.com/nikoladze/ahoi, 2018.

[250] ATLAS Collaboration, "Object-based missing transverse momentum significance in the ATLAS detector," Tech. Rep. ATLAS-CONF-2018-038, CERN, Geneva, Jul, 2018. https://cds.cern.ch/record/2630948.

[251] A. Roodman, "Blind analysis in particle physics," *eConf* **C030908** (2003) TUIT001, arXiv:physics/0312102.

[252] W. Buttinger, "Using Event Weights to account for differences in Instantaneous Luminosity and Trigger Prescale in Monte Carlo and Data," tech. rep., CERN, Geneva, May, 2015. https://cds.cern.ch/record/2014726.

[253] ATLAS Collaboration, "Measurement of the Inelastic Proton–Proton Cross Section at $\sqrt{s}$ = 13 TeV with the ATLAS Detector at the LHC," *Phys. Rev. Lett.* **117** (2016) 182002, arXiv:1606.02625 [hep-ex].

[254] ATLAS Collaboration, "A method for the construction of strongly reduced representations of ATLAS experimental uncertainties and the application thereof to the jet energy scale." ATL-PHYS-PUB-2015-014, 2015. https://cds.cern.ch/record/2037436.

[255] J. Bellm *et al.*, "Herwig 7.0/Herwig++ 3.0 release note," *Eur. Phys. J.* **C76** no. 4, (2016) 196, arXiv:1512.01178 [hep-ph].

[256] ATLAS Collaboration, "Simulation of top-quark production for the ATLAS experiment at $\sqrt{s}$ = 13 TeV." ATL-PHYS-PUB-2016-004, 2016. https://cds.cern.ch/record/2120417.

[257] S. Frixione, E. Laenen, P. Motylinski, *et al.*, "Single-top hadroproduction in association with a W boson," *JHEP* **07** (2008) 029, arXiv:0805.3067 [hep-ph].

[258] ATLAS Collaboration, "SUSY July 2020 Summary Plot Update," Tech. Rep. ATL-PHYS-PUB-2020-020, CERN, Geneva, Jul, 2020. http://cds.cern.ch/record/2725258.

[259] CMS Collaboration, "Search for chargino-neutralino production in final states with a Higgs boson and a W boson," Tech. Rep. CMS-PAS-SUS-20-003, CERN, Geneva, 2021. https://cds.cern.ch/record/2758360.

[260] ATLAS Collaboration, "Search for electroweak production of charginos and sleptons decaying into final states with two leptons and missing transverse momentum in $\sqrt{s}$ = 13 TeV pp collisions using the ATLAS detector," *Eur. Phys. J. C* **80** (2020) 123, arXiv:1908.08215 [hep-ex].

[261] G. Apollinari, I. Béjar Alonso, O. Brüning, *et al.*, *High-Luminosity Large Hadron Collider (HL-LHC): Preliminary Design Report*. CERN Yellow Reports: Monographs. CERN, Geneva, 2015. https://cds.cern.ch/record/2116337.

[262] X. Chen, S. Dallmeier-Tiessen, R. Dasler, *et al.*, "Open is not enough," *Nature Physics* **15** no. 2, (Feb, 2019) 113–119. https://doi.org/10.1038/s41567-018-0342-2.

[263] LHC Reinterpretation Forum Collaboration, W. Abdallah *et al.*, "Reinterpretation of LHC Results for New Physics: Status and Recommendations after Run 2," *SciPost Phys.* **9** no. 2, (2020) 022, arXiv:2003.07868 [hep-ph].

[264] ATLAS Collaboration, "RECAST framework reinterpretation of an ATLAS Dark Matter Search constraining a model of a dark Higgs boson decaying to two b-quarks." ATL-PHYS-PUB-2019-032, 2019. https://cds.cern.ch/record/2686290.

[265] K. Cranmer and I. Yavin, "RECAST: Extending the Impact of Existing Analyses," *JHEP* **04** (2011) 038, arXiv:1010.2506 [hep-ex].

[266] D. Dercks, N. Desai, J. S. Kim, *et al.*, "CheckMATE 2: From the model to the limit," *Comput. Phys. Commun.* **221** (2017) 383–418, arXiv:1611.09856 [hep-ph].

[267] M. Drees, H. Dreiner, D. Schmeier, *et al.*, "CheckMATE: Confronting your Favourite New Physics Model with LHC Data," *Comput. Phys. Commun.* **187** (2015) 227–265, arXiv:1312.2591 [hep-ph].

[268] E. Conte, B. Fuks, and G. Serret, "MadAnalysis 5, A User-Friendly Framework for Collider Phenomenology," *Comput. Phys. Commun.* **184** (2013) 222–256, arXiv:1206.1599 [hep-ph].

[269] E. Maguire, L. Heinrich, and G. Watt, "HEPData: a repository for high energy physics data," *J. Phys. Conf. Ser.* **898** no. 10, (2017) 102006, arXiv:1704.05473 [hep-ex].

[270] ATLAS Collaboration, "Simpleanalysis." https://gitlab.cern.ch/atlas-sa/simple-analysis, 2021.

[271] S. Ovyn, X. Rouby, and V. Lemaitre, "DELPHES, a framework for fast simulation of a generic collider experiment," arXiv:0903.2225 [hep-ph].

[272] A. Buckley, J. Butterworth, D. Grellscheid, *et al.*, "Rivet user manual," *Comput. Phys. Commun.* **184** (2013) 2803–2819, arXiv:1003.0694 [hep-ph].

[273] A. Buckley, D. Kar, and K. Nordström, "Fast simulation of detector effects in Rivet," *SciPost Phys.* **8** (2020) 025, arXiv:1910.01637 [hep-ph].

[274] S. Kraml, S. Kulkarni, U. Laa, *et al.*, "SModelS: a tool for interpreting simplified-model results from the LHC and its application to supersymmetry," *Eur. Phys. J. C* **74** (2014) 2868, arXiv:1312.4175 [hep-ph].

[275] F. Ambrogi, S. Kraml, S. Kulkarni, *et al.*, "SModelS v1.1 user manual: Improving simplified model constraints with efficiency maps," *Comput. Phys. Commun.* **227** (2018) 72–98, arXiv:1701.06586 [hep-ph].

[276] ATLAS Collaboration, "Search for direct production of electroweakinos in final states with one lepton, missing transverse momentum and a higgs boson decaying into two b-jets in pp collisions at $\sqrt{s}$ = 13 tev with the atlas detector," 2021. https://www.hepdata.net/record/ins1755298?version=4.

[277] ATLAS Collaboration, "1lbb-likelihoods-hepdata.tar.gz," 2020. https://www.hepdata.net/record/resource/1408476?view=true.

[278] G. Alguero, S. Kraml, and W. Waltenberger, "A SModelS interface for pyhf likelihoods," arXiv:2009.01809 [hep-ph].

[279] M. D. Goodsell, "Implementation of the ATLAS-SUSY-2019-08 analysis in the MadAnalysis 5 framework (electroweakinos with a Higgs decay into a $b\bar{b}$ pair, one lepton and missing transverse energy; 139 fb^{-1})," *Mod. Phys. Lett. A* **36** no. 01, (2021) 2141006.

[280] J. Y. Araz *et al.*, "Proceedings of the second MadAnalysis 5 workshop on LHC recasting in Korea," *Mod. Phys. Lett. A* **36** no. 01, (2021) 2102001, arXiv:2101.02245 [hep-ph].

[281] M. Feickert, L. Heinrich, G. Stark, and B. Galewsky, "Distributed statistical inference with pyhf enabled through funcX," in *25th International Conference on Computing in High-Energy and Nuclear Physics*. 3, 2021. arXiv:2103.02182 [cs.DC].

[282] R. Chard, Y. Babuji, Z. Li, *et al.*, "funcx: A federated function serving fabric for science," ACM, Jun, 2020. http://dx.doi.org/10.1145/3369583.3392683.

[283] D. Merkel, "Docker: Lightweight linux containers for consistent development and deployment," *Linux J.* **2014** no. 239, (Mar., 2014) .

[284] S. Binet and B. Couturier, "docker & HEP: Containerization of applications for development, distribution and preservation," *J. Phys.: Conf. Ser.* **664** no. 2, (2015) 022007. 8 p. https://cds.cern.ch/record/2134524.

[285] K. Cranmer and L. Heinrich, "Yadage and Packtivity - analysis preservation using parametrized workflows," *J. Phys. Conf. Ser.* **898** no. 10, (2017) 102019, arXiv:1706.01878 [physics.data-an].

[286] E. R. Gansner and S. C. North, "An open graph visualization system and its applications to software engineering," *SOFTWARE - PRACTICE AND EXPERIENCE* **30** no. 11, (2000) 1203–1233.

[287] E. R. Gansner, Y. Koren, and S. North, "Graph drawing by stress majorization," in *Graph Drawing*, J. Pach, ed., pp. 239–250. Springer Berlin Heidelberg, Berlin, Heidelberg, 2005.

[288] ATLAS Collaboration, "Electron and photon energy calibration with the ATLAS detector using 2015–2016 LHC proton–proton collision data," *JINST* **14** (2019) P03017, arXiv:1812.03848 [hep-ex].

[289] Schanet, Eric, "simplify," Version 0.1.5. https://github.com/eschanet/simplify.

[290] Schanet, Eric, "SUSY-2019-08 simplified likelihood," Version 0.0.1. https://github.com/eschanet/simplify/blob/master/examples/ANA-SUSY-2019-08/simplify_BkgOnly.json.

[291] P. C. Bryan and M. Nottingham, "Javascript object notation (json) patch," Version RFC 6902, Apr, 2013. https://www.rfc-editor.org/rfc/rfc6902.txt.

[292] ATLAS Collaboration, "Search for direct stau production in events with two hadronic τ-leptons in $\sqrt{s} = 13$ TeV pp collisions with the ATLAS detector," *Phys. Rev. D* **101** (2020) 032009, arXiv:1911.06660 [hep-ex].

[293] ATLAS Collaboration, "Search for bottom-squark pair production with the ATLAS detector in final states containing Higgs bosons, b-jets and missing transverse momentum," *JHEP* **12** (2019) 060, arXiv:1908.03122 [hep-ex].

[294] W. Porod, "SPheno, a program for calculating supersymmetric spectra, SUSY particle decays and SUSY particle production at e+ e- colliders," *Comput. Phys. Commun.* **153** (2003) 275–315, arXiv:hep-ph/0301101.

[295] W. Porod and F. Staub, "SPheno 3.1: Extensions including flavour, CP-phases and models beyond the MSSM," *Comput. Phys. Commun.* **183** (2012) 2458–2469, arXiv:1104.1573 [hep-ph].

[296] S. Heinemeyer, W. Hollik, and G. Weiglein, "FeynHiggs: A Program for the calculation of the masses of the neutral CP even Higgs bosons in the MSSM," *Comput. Phys. Commun.* **124** (2000) 76–89, arXiv:hep-ph/9812320.

[297] H. Bahl, T. Hahn, S. Heinemeyer, *et al.*, "Precision calculations in the MSSM Higgs-boson sector with FeynHiggs 2.14," *Comput. Phys. Commun.* **249** (2020) 107099, arXiv:1811.09073 [hep-ph].

[298] T. Hahn, S. Heinemeyer, W. Hollik, *et al.*, "High-Precision Predictions for the Light CP -Even Higgs Boson Mass of the Minimal Supersymmetric Standard Model," *Phys. Rev. Lett.* **112** no. 14, (2014) 141801, arXiv:1312.4937 [hep-ph].

[299] B. C. Allanach, "SOFTSUSY: a program for calculating supersymmetric spectra," *Comput. Phys. Commun.* **143** (2002) 305–331, arXiv:hep-ph/0104145 [hep-ph].

[300] G. Belanger, F. Boudjema, A. Pukhov, and A. Semenov, "MicrOMEGAs 2.0: A Program to calculate the relic density of dark matter in a generic model," *Comput. Phys. Commun.* **176** (2007) 367–382, arXiv:hep-ph/0607059.

[301] G. Belanger, F. Boudjema, A. Pukhov, and A. Semenov, "micrOMEGAs: A Tool for dark matter studies," *Nuovo Cim. C* **033N2** (2010) 111–116, arXiv:1005.4133 [hep-ph].

[302] W. Beenakker, R. Hopker, and M. Spira, "PROSPINO: A Program for the Production of Supersymmetric Particles in Next-to-leading Order QCD," Tech. Rep. hep-ph/9611232, Nov, 1996. https://cds.cern.ch/record/314229. 12 pages, latex, no figures, Complete postscript file and FORTRAN source codes available from http://wwwcn.cern.ch/ mspira/prospino/.

[303] W. Beenakker, M. Klasen, M. Kramer, *et al.*, "The Production of charginos / neutralinos and sleptons at hadron colliders," *Phys. Rev. Lett.* **83** (1999) 3780–3783, arXiv:hep-ph/9906298. [Erratum: Phys.Rev.Lett. 100, 029901 (2008)].

[304] ATLAS Collaboration, "Search for long-lived charginos based on a disappearing-track signature using 136 fb^{-1} of pp collisions at $\sqrt{s}$ = 13 TeV with the ATLAS detector," Tech. Rep. ATLAS-CONF-2021-015, CERN, Geneva, Mar, 2021. https://cds.cern.ch/record/2759676.

[305] A. Arbey, M. Battaglia, and F. Mahmoudi, "Higgs Production in Neutralino Decays in the MSSM - The LHC and a Future e^+e^- Collider," *Eur. Phys. J. C* **75** no. 3, (2015) 108, arXiv:1212.6865 [hep-ph].

[306] M. E. Cabrera, J. A. Casas, A. Delgado, *et al.*, "Naturalness of MSSM dark matter," *JHEP* **08** (2016) 058, arXiv:1604.02102 [hep-ph].

[307] N. Arkani-Hamed, G. L. Kane, J. Thaler, and L.-T. Wang, "Supersymmetry and the LHC inverse problem," *JHEP* **08** (2006) 070, arXiv:hep-ph/0512190.

[308] S. Amari, *Differential-Geometrical Methods in Statistics.* Springer New York, New York, NY, 1985.

[309] J. Brehmer, K. Cranmer, F. Kling, and T. Plehn, "Better Higgs boson measurements through information geometry," *Phys. Rev. D* **95** no. 7, (2017) 073002, arXiv:1612.05261 [hep-ph].